Woodsmoke particle exposure prior to SARS-CoV-2 infection alters antiviral response gene expression in human nasal epithelial cells in a sex-dependent manner

Woodsmoke in nasal epithelial response to SARS-CoV-2

Authors:

Stephanie A. Brocke[1], Grant T. Billings[2], Sharon Taft-Benz[3], Neil E. Alexis[4], Mark T. Heise[3,5], Ilona Jaspers[1,4]*

* Corresponding author: ilona_jaspers@med.unc.edu

116 Manning Dr. 4310 Mary Ellen Jones Bldg., Chapel Hill, NC 27599

Affiliations:

1 Curriculum in Toxicology and Environmental Medicine, University of North Carolina, Chapel Hill, NC

2 Crop and Soil Sciences Department, North Carolina State University, Raleigh, NC

3 Department of Genetics, University of North Carolina School of Medicine, Chapel Hill, NC

4 Center for Environmental Medicine, Asthma, and Lung Biology, University of North Carolina, Chapel Hill, NC

5 Department of Microbiology and Immunology, University of North Carolina, Chapel Hill, NC

Supplemental Material available at: https://doi.org/10.6084/m9.figshare.16413261.v1

Abstract:

Inhalational exposure to particulate matter (PM) derived from natural or anthropogenic sources alters gene expression in the airways and increases susceptibility to respiratory viral infection. Woodsmoke-derived ambient PM from wildfire events during 2020 was associated with higher COVID-19 case rates in the western US. We hypothesized that exposure to suspensions of woodsmoke particles (WSP) or diesel exhaust particles (DEP) prior to SARS-CoV-2 infection would alter host immune gene expression at the transcript level. Primary human nasal epithelial cells (hNECs) from both sexes were exposed to WSP or DEP (22 μg/cm^2) for 2 h, followed by infection with SARS-CoV-2 at a multiplicity of infection of 0.5. Forty-six genes related to SARS-CoV-2 entry and host response were assessed. Particle exposure alone minimally affected gene expression, while SARS-CoV-2 infection alone induced a robust transcriptional response in hNECs, upregulating type I and

III interferons, interferon-stimulated genes, and chemokines by 72 h p.i. This upregulation was higher overall in cells from male donors. However, exposure to WSP prior to infection dampened expression of antiviral, interferon, and chemokine mRNAs. Sex-stratification of these results revealed that WSP exposure downregulated gene expression in cells from females more so than males. We next hypothesized that hNECs exposed to particles would have increased apical viral loads compared to unexposed cells. While apical viral load was correlated to expression of host response genes, viral titer did not differ between groups. These data indicate that WSP alter epithelial immune responses in a sex-dependent manner, potentially suppressing host defense to SARS-CoV-2 infection.

Author Contributions:

IJ, SAB, and MTH conceived and designed the study; SAB and STB performed experimentation and collection of data; GTB and SAB were involved in data processing, analysis, and visualization; SAB, IJ, and NEA conceptualized the manuscript; SAB and IJ drafted the manuscript; SAB, NEA, and IJ provided critical revision of the manuscript and interpretation of findings; SAB, GTB, STB, NEA, MTH, and IJ approved the final version of the manuscript.

Keywords:

Woodsmoke, particulate matter (PM), sex difference, nasal epithelium, antiviral defense, SARS-CoV-2 host response

Introduction

Wildfires contribute significantly to air pollution and ambient particulate matter (PM) (1, 2). During the 2020 fire season, large, populous regions of the western United States were exposed to unhealthy or hazardous air quality from woodsmoke-derived PM (3). Studies have shown that wildland firefighters can be exposed to respirable particulate matter at concentrations >1 mg/m^3 over the course of their work shift with maximum exposures reaching >2.5 mg/m^3 (4-6). Particulate air pollution released from burning wildlands is associated with negative respiratory and cardiovascular health outcomes (reviewed in (7-10)) the toxicity of which depends heavily on the type of biomass burned and the burn temperature (11). Epidemiological studies examining the health effects of wildfires showed an association between PM from wildfires and increased respiratory hospitalizations across 16 western states (12). A similar health effects study in California showed that women were more likely than men to visit the hospital for asthma- or hypertension-related reasons due to an increase in wildfire-generated PM (13), suggesting sex-dependent effects.

Coinciding with severe wildfires was the global coronavirus disease 2019 (COVID-19) pandemic that is, to date, responsible for over 4.9 million deaths worldwide (14). Sex has been found to affect COVID-19 outcomes with males more likely than females to develop severe or fatal cases of the disease (15-17). SARS-CoV-2, the etiologic agent behind COVID-19, primarily affects the respiratory system (18) and exhibits tropism for cells of the upper airways, with nasal epithelial cells most susceptible to infection (19). Primary human nasal epithelial cells (hNECs) grown *in vitro* at air-liquid interface mimic *in vivo* differentiation patterns, evidenced by expression of mucins, presence of beating cilia, and tight junction formation (20, 21). Because the nasal epithelium expresses the SARS-CoV-2 viral entry factors angiotensin converting enzyme 2 (ACE2) and transmembrane serine protease 2 (TMPRSS2) in ciliated and secretory cells (22), the differentiated hNEC model is a suitable *in vitro* culture system to study SARS-CoV-2 pathogenesis. Along with biological aerosols, the nasal epithelium is exposed to airborne particulates, gaseous pollution, and allergens *in vivo*. Thus, in addition to being a useful model for studying respiratory viral infection (23, 24), hNECs demonstrate utility for toxicological studies involving aerosolized (25, 26) and gaseous (27) toxicants.

Exposure to air pollution is known to alter susceptibility to respiratory viral infection (reviewed in (28, 29)). *In vitro* models of respiratory epithelium treated with diesel exhaust particles (DEP) prior to influenza infection demonstrated increases in viral attachment and the number of virus-infected cells relative to untreated cells

(23). Red oak woodsmoke exposure followed by live attenuated influenza virus (LAIV) inoculation suppressed expression of host defense genes in women and upregulated many pro-inflammatory genes in men (30). Numerous epidemiological studies from around the world have found correlations between ambient air pollution levels and COVID-19 case number or case fatality rate (31-35). Recently, two studies found positive associations between ambient woodsmoke particles (WSP) and COVID-19 cases and deaths in the western United States (36, 37).

The present study examined the interactive effects of sex, exposure to WSP, and SARS-CoV-2 infection on gene expression in hNECs. To do this, hNECs from male and female healthy human donors were exposed to aqueous suspensions of DEP or WSP derived from burned eucalyptus or red oak. Particle exposures occurred prior to and during infection with SARS-CoV-2 and sampling occurred at 0, 24, and 72 h post infection (p.i.). We measured expression of a panel of 46 genes related to respiratory viral infection and host immune response, including the SARS-CoV-2 entry factor (*ACE2*), several airway proteases, interferons, interferon-stimulated genes (ISGs), chemokines, transcription factors, pathogen recognition receptors, mucins, and surfactants. Additionally, the effects of particle exposure on viral load were assessed by measuring viral titers in apical washes collected from hNECs in the various exposure groups.

Methods

Primary Nasal Epithelial Cell Donors

Collection of primary hNECs from adults was performed as previously described (21). Superficial nasal epithelial scrape biopsies were obtained from healthy, non-smoking male and female adults with a Rhino-Pro curette (Arlington Scientific, Inc. 96-0900) per protocols approved by the University of North Carolina School of Medicine Institutional Review Board for Biomedical Research (protocol numbers 05-2528, 09-0716, 11-1363). Written informed consent was obtained from all study participants. HNECs from an equal number of male and female donors were used for each experiment. Demographic information about the donors used for each exposure including age, BMI, and race is provided in Table 1. Nasal biopsies were stored in RPMI-1640 medium (Gibco 11875-093) on ice until further processing.

Expansion and Culture of hNECs

Culture of hNECs was performed as previously described (21, 26). Cells from nasal biopsy were expanded at passage 0 on a 12-well, PureCol-coated (Advanced Biomatrix 5005-100ML) cell culture plate (Costar 3512) in

PneumaCult -Ex Plus Medium (Stemcell Technologies 05041, 05042) supplemented with hydrocortisone (Stemcell Technologies 07925), antibiotic antimycotic solution (Sigma A5955), and gentamicin reagent solution (Gibco 15750-060). Cells were passaged and further expanded in 25 cm^2 tissue culture flasks (Corning 430639) until passage 2. HNECs were then seeded on 12 mm transwell inserts with 0.4 µm pores (Costar 3460) coated with human placental collagen (Sigma C7521-10MG) at a density of 203,000-333,000 cells per well and maintained in PneumaCult -Ex Plus Medium. Once confluency was reached on the transwells, the cultures were taken to air-liquid-interface (ALI) and the apical medium was permanently removed, while the basolateral medium was switched for PneumaCult ALI Medium (Stemcell Technologies 05002, 05003, 05006), supplemented with 1% pen strep (Gibco 15140-122), hydrocortisone (Stemcell Technologies 07925), and heparin (Stemcell Technologies 07980). After this point, three times per week the basolateral medium was changed and the apical surfaces of the cultures were washed with 37°C HBSS + $CaCl_2$, + $MgCl_2$ (HBSS++) (Gibco 14025-092). Mucociliary differentiation of the cultures was achieved after 4-6 weeks of ALI conditions. At the time of exposure, cultures were at ALI for 5.29-9.14 weeks.

Diesel Exhaust Particle (DEP) Suspension Preparation

Whole diesel exhaust particle material from an automobile engine was collected as described by Sagai, et al. (38). The DEP were generated using an Isuzu Automobile Co. 4JB1-type light duty 4 cylinder diesel engine (2740cc). The engine was operated under a load of 6 kg-m of torque at 2000 RPM. Particles were collected "cold" at a sampling temperature of 50°C from glass fiber filters and the stainless-steel walls of the collection duct (38). Twenty-five mg of the DEP was diluted in 5 ml of warmed (37°C) phenol red-free MEM basal medium (Gibco 51200-038). The suspension was sonicated with a Fisher Sonic Dismembrator Model 500 with a microprobe tip for two 1-minute cycles. During each cycle the probe was moved up and down in the suspension, and sonication alternated between 30% output for 0.5 s and 0% output for 0.5 s. After each cycle, the suspension was mixed by inversion. An additional 20 ml of warmed (37°C) medium was then added to the suspension to achieve a final concentration of 1 mg/ml. Aliquots of the suspension were snap frozen in liquid nitrogen and stored at -80°C for future use.

Woodsmoke Particle (WSP) Suspension Preparation

Woodsmoke generated from eucalyptus (*Eucalyptus globulus*) and red oak (*Quercus rubra*) were each collected as previously described by Kim, et al. (11). Briefly, eucalyptus or red oak were burned in a quartz

tube furnace at 640°C and smoke was collected in a series of cryogenic traps. The resulting woodsmoke particle condensates were then collected in acetone and concentrated with a rotary evaporator. Finally, the particles were dried and the solid PM was resuspended in Dulbecco's PBS (Gibco 14200-075) at 2 mg/ml and frozen at -20°C. Prior to exposure, aliquots were sonicated in a water bath sonicator (Sinosonic Industrial Co. Ltd., Taiwan, Model B200) at 40 KHz for 4.75 min.

Particle Size Measurements

Chemical composition analyses of particles used here from previously published studies are presented in Supplemental Table S1. Particle size distributions of the three particle suspensions were determined by diluting an aliquot of each to 50 µg/ml in ddH_2O. The diluted suspensions were run through a BD FACSVerse 2013 Flow Cytometer for size measurement and compared to size calibration standards (Thermo Fisher F13838) of 1.0, 2.0, 4.0, 6.0, 10.0, and 15.0 µm in diameter. Graphs of particle size distribution overlaid with the standard sizes are shown in Supplemental Fig. S1.

Exposure of hNECs to DEP or WSP

A pictorial depiction of the exposure and infection scheme is provided in Fig. 1. Prior to exposure, the apical surface of each culture was washed with 100 µl of warmed (37°C) HBSS++ and basolateral medium was replaced with 1.0 ml of 37°C PneumaCult ALI Medium. Warm ALI Medium was used as the control exposure and as the vehicle for particle exposures. HNECs from three male and three female donors were used for each type of exposure (DEP, eucalyptus WSP, and red oak WSP). Separate cultures from the same donor were used in multiple groups in some cases. Particle stock aliquots were diluted in ALI medium and applied to the apical surface of the experimental wells at a concentration of 165.7 µg/ml in 150 µl apical volume. This corresponds to a dosage of 22 µg/cm^2, which we have studied previously (23). Control wells received 150 µl ALI medium apically. Cultures were then returned to the incubator (37°C, 5% CO_2) for 2 h.

Infection with SARS-CoV-2 or Mock

At the end of the 2-h exposure, half the wells exposed to particle and half the control wells were apically infected with SARS-CoV-2 derived from clinical isolate WA1 (19) in high glucose DMEM (Gibco 11995-065) with 5% heat-inactivated fetal bovine serum, 1% L-glutamine diluted in ALI medium at a M.O.I. (multiplicity of infection) of 0.5 in 100 µl. The other half of the cultures were mock infected with 100 µl of high glucose DMEM with 5% heat-inactivated fetal bovine serum, 5% L-glutamine diluted in ALI medium. To avoid damaging or

disturbing the cell monolayer, particle suspensions were not removed before addition of viral inoculum or vehicle. Total apical volume during viral infection was thus 250 ul. Cultures were then returned to the incubator (37°C, 5% CO_2) for 2 h.

Sample Collection

After the 2-h infection, cells were checked under the microscope for signs of cell death. The apical liquid was carefully removed from every well. Cultures were then washed with 200 µl 37°C HBSS++ and returned to the incubator until collection. At the time of collection (0, 24, or 72 h p.i.), 100 µl 37°C HBSS++ was added to the apical surface of each culture, and cells were returned to the incubator for 15 min. Apical washes were then carefully collected and analyzed for viral titer. Cells were lysed using 350 µl cold TRIzol reagent (Life Technologies 15596018) for subsequent gene expression analysis.

Determination of Viral Titer

Fifty microliters of the apical wash were mixed with 450 µl of medium (DMEM + 5% FBS + 1% L-glutamine) followed by ten-fold serial dilutions resulting in a dilution series of 10^{-1} to 10^{-6}. Two hundred µl of each dilution was added to plated Vero E6 cells (C1008, ATCC) and incubated at 37°C. Plates were rocked every 15 min to ensure even distribution of the virus over the surface of the well. After 1 h, 2 ml of overlay (50:50 mixture of 2.5% carboxymethylcellulose and 2X alpha MEM containing 6% FBS + 2% penicillin/streptomycin + 2% L-glutamine + 2% HEPES) was added to each well. Plates were incubated at 37°C, 5% CO_2 for 4 days, then fixed with 2 ml of 4% paraformaldehyde left on overnight. Following removal of the fixative, wells were rinsed with water to remove residual overlay and then stained with 0.25% crystal violet. Visible plaques were counted and averaged between two technical replicate wells. Viral titers were calculated as plaque forming units (pfu) per ml. The limit of detection for the assay was determined to be 12.5 pfu / wash, and samples that yielded no plaques were assigned a value of 6.25, half of the limit of detection.

RNA extraction from whole cell lysates in TRIzol

Whole cell lysates in TRIzol reagent were thawed on ice. An additional 650 µl cold TRIzol was added to each sample to facilitate RNA collection. Two hundred µl chloroform was added to each tube and tubes were shaken vigorously and incubated at room temperature for 3 min. Samples were then centrifuged for 15 min at 12,000 x g at 4°C. The aqueous phase containing RNA was then carefully removed from each sample and transferred to new microcentrifuge tubes. One volume of 100% ethanol was added per volume of aqueous

phase removed and samples were vortexed. Samples were further processed with the Zymo RNA Clean and Concentrator Kit (Zymo R1016) according to the manufacturer's instructions. Eluted RNA was stored at -80°C until use.

Generation of cDNA and Quantification of Gene Expression of 48 genes by qPCR

RNA concentration and purity were measured using a CLARIOstar plate reader and an LVis Plate (BMG LABTECH). For each sample, 800 ng of RNA was used to generate cDNA in a reaction volume of 25 µl. The final concentrations of reagents in each reaction were as follows: 0.50 mM dNTPs (Promega U151B), 1.00 U/µl RNasin Ribonuclease Inhibitor (Promega N211A), 10.0 U/µl M-MLV Reverse Transcriptase (Invitrogen 28025-013), 0.10 µg/µl Random Primers (Invitrogen 58875), 50.0 mM KCl, 0.25 mM $MgCl_2$, 20.0 mM Tris-HCl, 0.01 mg/ml BSA. PCR was performed in 96-well plates (Thermo AB-0600, AB-0851) for one cycle (25.0°C for 10 min, 37.0°C for 50 min, 70.0°C for 15 min, followed by 4.0°C infinite hold). Samples were submitted to the UNC School of Medicine Center for Gastrointestinal Biology and Disease Advanced Analytics Core for high-throughput qPCR gene expression analysis. Gene expression of a panel of 48 genes (including 2 reference genes) was assayed in a Fluidigm BioMark HD system using TaqMan primers and probes (Table 2). Duplicate Ct values were measured for each sample/gene combination and averaged for further analysis. Gene expression was calculated using the ΔΔCt method with normalization to the geometric mean of expression of the two reference genes (*ACTB* and *GAPDH*). Two samples (out of 216) showing poor amplification across the panel (i.e. comparable to the no-template controls) were excluded from the data set and not further analyzed.

Quantification of SARS-CoV-2 N1 and N2 gene expression by qPCR

Expression of viral SARS-CoV-2 N1 and N2 genes was also quantified and normalized to human RNase P gene expression using the Integrated DNA Technologies 2019-nCoV RUO Kit (IDT 10006713). For a single reaction, 6.5 µl nuclease-free water, 1.5 µl of one primer/probe mix, and 10 µl of TaqMan Universal Master Mix II, with UNG (Thermo Fisher 4440038) were mixed and added to every well of a Sapphire 96-well PCR Microplate (Greiner Bio-one 652260). cDNA was then added to each well (2 µl) for a total volume of 20 µl per reaction. The plate was sealed with a plate film (Thermo Fisher 4311971) and centrifuged for 5 min at 500 x g at room temperature. RT-qPCR was performed on a QuantStudio 3 using the following reaction conditions: hold 50.0°C for 2 min then hold 95.0°C for 10 min, cycle through 95.0°C for 15 s and 60.0°C for 1 min for 40 cycles. Transitions between temperatures occurred at 1.6°C/s. The two samples excluded from the Fluidigm

PCR data were also excluded here. Results were collected as Ct and analyzed with the ΔΔCt method, normalized to expression of human RNase P.

Statistical Analysis

Analysis was carried out using SAS PROC MIXED as a full factorial design, with sex (M or F), particle treatment (control, DEP, eucalyptus WSP, or red oak WSP), virus or no virus, and duration (0, 24, or 72 h), as well as all their interactions. Donor was fit as a random effect. Preplanned hypothesis tests for differences between marginal means were carried out as t-tests with the LSMESTIMATE command. Sex-specific means were calculated for each combination of particle treatment, virus, and duration and differences were tested using a t-test with the LSMESTIMATE command. Correction for multiple comparisons was performed across all statistical tests for the entire experiment using the 'qvalue' R package (v. 2.22.0), with a false discovery rate q-value threshold of 0.05, assuming pi0 = 1 (equivalent to Benjamini-Hochberg correction). The resultant p-value for statistical significance was $p \leq 0.00369$. Viral titer data were analyzed using GraphPad Prism v. 8.4.0. Unpaired t-tests (with Welch's correction when appropriate) were used to evaluate differences in $\log_{10}$-transformed data.

Results

Particle exposure alone has modest effects on expression of antiviral host response genes

First, we assessed how exposure to particles alone without subsequent viral infection would affect expression of host response genes in our panel. HNECs from male and female donors were exposed to one of three particle suspensions (DEP, eucalyptus WSP, or red oak WSP) or control for 2 h, followed by a "mock" infection for 2 h. Results are shown graphically in Fig. 2 and statistically significant results are reported in Table 3. At 0 h post mock infection, exposure to both types of WSP increased expression of *IL6* and eucalyptus WSP also upregulated expression of *IL1B*. Further, DEP and red oak WSP significantly decreased expression of *IFNG* at 0 h p.i. (data for eucalyptus WSP not shown due to missing data points). By 24 h p.i. both eucalyptus WSP and red oak WSP further upregulated *IL1B* expression, while *IL6* was no longer upregulated. Overall, by 24 and 72 h p.i., particle treatment in the absence of infection had little effect on expression of the genes in our panel.

SARS-CoV-2 infection greatly affects expression of antiviral host response genes in hNECs

In order to assess how particle exposure affects expression of antiviral host defense genes in the presence of an infection, we next needed to measure the independent effects of SARS-CoV-2 infection on gene expression.

Thus, hNECs from male and female donors which were not exposed to any particles were infected with SARS-CoV-2 (or mock infected with vehicle). Virus-induced changes in gene expression in hNECs at 0, 24, and 72 h p.i. are shown in Fig. 3 and fold-inductions and p-values are tabulated in Table 4. By 24 h p.i., the Type III IFNs (*IFNL1* and *IFNL2*) were upregulated in hNECs from male and female donors, with statistically significant upregulation of both genes in males. Expression of *IFNL1* and *IFNL2* were even more highly upregulated at 72 h p.i. and reached statistical significance in both sexes. Additionally, by 72 h p.i., infection had upregulated mRNAs of type I interferons, ISGs, chemokines, transcription factors, and viral recognition receptors. In most instances, gene expression in hNECs from males was more highly induced by infection than in hNECs from females, suggesting an overall more robust epithelial response to SARS-CoV-2 in hNECs from male donors. For each gene that was differentially expressed in infected cells from both sexes, the ratio of expression in males:females was calculated. Indeed, on average the level of virus-induced gene expression in hNECs from males was 2.08 times (95% CI: ± 0.57) that of hNECs from females. We also assessed whether baseline differences in gene expression existed between the sexes in uninfected cells. There were no statistically significant differences in baseline gene expression between hNECs from males and females at 24 and 72 h post mock infection (data not shown).

Woodsmoke particles affect expression of virus-induced genes in hNECs infected with SARS-CoV-2

We hypothesized that exposure to particles would dampen expression of crucial antiviral host response genes upon subsequent SARS-CoV-2 infection. To test this, hNECs from male and female donors were exposed to control or DEP, eucalyptus WSP, or red oak WSP for 2 h, followed by infection with SARS-CoV-2. Overall, red oak WSP caused more statistically significant changes in virus-induced gene expression than the other particles (Table 5). DEP had very few effects on virus-induced gene expression at all time points. In general, the number of statistically significant effects on gene expression increased with duration of infection in the WSP-exposed groups. More specifically, at 0 h p.i., both types of WSP increased *IL1B* and *IL6* expression compared to unexposed, infected cells, with red oak WSP exposure generating more potent upregulation of *IL6*. By 24 h p.i, all three types of particles upregulated *IL1B* to similar degrees and red oak WSP downregulated *MX1* and *STAT2*. At 72 h p.i. WSP exposures, especially from red oak, decreased expression of several genes, including *IFNB1*, *CCL3*, *CCL5, CXCL10*, and *CXCL11* (Fig. 4). Red oak WSP also decreased expression of *IFNL1* and *IFNL2*, albeit not statistically significantly. Other genes that are important

for the antiviral response group were also downregulated by WSP, such as *IFIT1*, *IFITM3*, *MX1*, *IRF7*, *STAT1*, *STAT2*, *DDX58*, and *MMP7*. Thus, exposure to WSP prior to infection with SARS-CoV-2 suppressed IFN-dependent immune gene expression.

Woodsmoke particle effects on gene expression in infected hNECs are sex-specific

Because the virus-induced effects on gene expression were sex-dependent (Fig. 3), we next assessed whether gene expression changes in cells exposed to particles prior to infection were also sex-dependent. Few sex-specific changes were observed at 0 and 24 h p.i. (Table 6). However, at 72 h p.i., WSP from eucalyptus and red oak modified virus-induced expression of more genes in hNECs from female donors than from male donors (Fig. 5). At this timepoint, WSP from both eucalyptus and red oak caused statistically significant downregulation of *IFITM3*, *MX1, IRF7*, and *STAT1* in hNECs from females. Additionally, red oak WSP caused a statistically significant decline in *MX1* expression in hNECs from females versus males. These results suggest that WSP exposure, especially from red oak, dampens expression of antiviral genes in hNECs from females during SARS-CoV-2 infection, with lesser effects on hNECS from males.

Particle exposure does not affect viral load in hNECs

Previously, we found that exposing hNECs and other airway epithelial cells to DEP prior to infection with influenza A enhanced viral replication and susceptibility to viral infection (23). Because WSP exposure altered expression of antiviral genes in the present study, we assessed whether viral replication and release were also altered by WSP exposure. Apical viral loads for the hNECs exposed to particles and their respective controls at 0, 24, and 72 h p.i. are shown in Fig. 6 A-C. The amount of infectious virus recovered from apical washes increased with duration of infection (Fig. 6 D), suggesting increased viral replication and apical secretion over time, consistent with our previous study (19). However, exposure to particles regardless of type had no effect on viral loads in apical washes (Fig. 6 A-D).

The relationship between the expression level of each gene (relative to reference genes) and the viral titer recovered from respective samples is shown in Fig. 7. As expected, expression levels of SARS-CoV-2 N1 and N2 genes are highly correlated with viral load recovered (Pearson's $r = 0.91$ for both). This indicates that apical release of infectious viral particles is highly correlated with viral mRNA levels. The following genes are also correlated with viral titer, with a statistically significant Pearson's $r > 0.70$: *ACE2*, *IFIT1*, *IFITM3*, *IFNB1*, *IFNL1*,

IFNL2, *MX1*, *CCL5*, *CXCL10*, *IRF7*, *STAT1*, *DDX58*, and *TLR9*. In contrast, *TMPRSS2* and *IL1B* both appear to be negatively correlated with viral titer.

Discussion

During 2020, air quality reached unhealthy and hazardous levels in the western United States due to wildfires which coincided with the spread of COVID-19. Epidemiological evidence has shown that worsened air quality from PM is associated with increased COVID-19 case rate and case fatality rate around the world (31-37, 39, 40). Toxicological studies have indicated that PM exposure affects the host defense response of the airways upon viral infection. In the present study, we hypothesized that exposing hNECs to PM derived from diesel exhaust and woodsmoke would alter the expression of host antiviral response genes upon subsequent infection with SARS-CoV-2. We also hypothesized that these effects would be sex-dependent.

Exposure to DEP or WSP in the absence of infection had few effects on expression of genes in our panel, besides upregulation of pro-inflammatory *IL6* and *IL1B* and downregulation of *IFNG.* Some studies of WSP exposure in human volunteers did not show significant pro-inflammatory changes in the airway (41-43) while others found signs of pulmonary or systemic inflammation following WSP exposure (6, 44). Pro-inflammatory effects of WSP on epithelial cells *in vitro* have been mild and inconsistent in past studies (45-47). These discrepancies could be due in part to differences in exposure paradigms, fuel types, and burn conditions across studies. Indeed, exposure to aerosolized particles versus particle suspensions alters the toxicological outcomes *in vitro (*48*).* Kim, et al. reported that both biomass fuel source and burn temperature affected chemical composition and thus toxicity of WSP in an *in vivo* mouse exposure (11). Additionally, particle size is an important consideration in *in vitro* exposures to particles. Pulmonary toxicity is thought to be inversely related to particle size since smaller particles have a higher surface area to mass ratio (49-51). Moreover particles differentially deposit in the respiratory tract based on particle size (52), which is another factor to be considered when modeling inhalational toxicity. As shown in Supplemental Fig. S1, there were differences in the particle size distributions for the DEP and WSP used in the present study, meaning different numbers of particles were delivered per unit mass in the three exposure groups. This should be acknowledged as a limitation to making direct comparisons between the effects induced by each of the three particle types. However, differences in chemical compositions of the particles (Supplemental Table S1) may also contribute to their differential effects. Computational clustering analyses have revealed certain chemical groups in biomass

smoke are linked to enhanced or repressed toxicity (53) and may therefore be an approach to further delineate which chemical signatures are drivers of the effects on antiviral host defense responses.

Our data indicate that SARS-CoV-2-induced gene expression changes in hNECs are sex-dependent, alone and in the context of WSP exposure (Fig. 3 and Fig. 5). In response to infection, expression of many of the genes in our panel increased, matching previously reported findings about the cellular responses to SARS-CoV-2 infection. Induction of type I and type III interferons is well-documented in the epithelial cell response to SARS-CoV-2 infection ((54, 55) reviewed in (56, 57)). We observed significant upregulation of *IFNB1*, *IFNL1*, and *IFNL2* mRNA by 72 h p.i., while *IFNA1* and *IFNA2* were not induced. Accordingly, several interferon-stimulated genes with antiviral function (*IFIT1*, *IFITM3*, *MX1*) and related transcription factors (*IRF1, IRF7*, *STAT1*, *STAT2*) (reviewed in (59)) were also induced in infected hNECs from one or both sexes. In addition to activating the interferon response pathway, SARS-CoV-2 is known to activate NF-κB transcription factors and result in upregulation of genes which promote leukocyte chemotaxis (55, 61), reviewed in (62-65). While in our model SARS-CoV-2 infection induced expression of many of these chemokines in both sexes, by 72 h p.i. hNECs from males displayed greater upregulation of antiviral and immune signaling gene expression than hNECs from females. In contrast, in our previous study examining nasal mucosal immune responses to inoculation with live attenuated influenza virus (LAIV) vaccine, Rebuli, et al. observed a more robust antiviral and inflammatory response in female subjects exposed to LAIV compared to male subjects (30). In that study, it was hypothesized that the seemingly larger upregulation of genes involved with antiviral defense and immune cell recruitment in females could reflect differential baseline gene expression levels between the sexes (30). However, in the data presented here, no differences in baseline gene expression were observed between the sexes at 24 and 72 h p.i. (data not shown). This previous *in vivo* human study also revealed that exposure to woodsmoke (500 $\mu g/m^3$) for 2 h prior to inoculation with LAIV resulted in upregulation of inflammatory gene expression in males and suppression of antiviral defense genes in females (30). The data presented here showed a similar, sex-dependent response to woodsmoke exposure in the context of infection. It is worth noting that the particles used in our study were not removed from the cells prior to addition of the virus, however we do not expect they interfered with viral infection since apical viral loads and viral gene expression did not differ between exposed and unexposed groups. Suppression of genes involved in the interferon response pathway was more frequent and greater in magnitude in hNECs from females versus males treated

with WSP before SARS-CoV-2 infection. Signaling molecules involved in recruitment of immune cells were also generally more downregulated in hNECs from females compared to males. These findings suggest that WSP exposure may dampen antiviral responses in females. Furthermore, since many of the genes assayed in this study are involved in general antiviral host defense, these results may translate to other viral pathogens of public health importance. Recently, urban PM was shown to impair antiviral properties of airway epithelial cultures towards SARS-CoV-2 and 229E-CoV, which causes the common cold (66).

Although our data did not show significant differences in viral titers based on sex or particle exposure, gene expression correlated significantly with viral titers and uncovered positive and negative associations with immune and inflammatory genes. Several of these positive correlations to antiviral genes (i.e. *IFNB1*, *IFNL1*, *IFNL2*, *IFIT1*, *IFITM3*, *ACE2*, *MX1*, *STAT1*, *DDX58*, and *CXCL10*) have been previously reported (54, 55). Expression of *TMPRSS2,* a protease which is crucial for SARS-CoV-2 entry (67), was negatively correlated with viral titer, which was also shown by Lieberman, et al. (55). Interestingly, *IL1B* expression was negatively correlated with viral titer in our model, and expression of *IL6*, *TNF*, and *CXCL8* showed weak positive or no associations with viral titer (r of 0.42, 0.14, and 0.28 respectively). These findings may be indicative of viral evasion of pro-inflammatory cytokine induction but indicate that the gene expression response to SARS-CoV-2 infection in our nasal epithelial model is dominated by the IFN response.

The fact that there were no differences in viral load recovered from exposed and unexposed hNECs, even at 72 h p.i., points at some potential limitations of the data presented here. The first is that the changes observed in gene expression at the transcript level may not translate into functional differences at the tissue level. Although *IFIT1*, *IFITM3*, *IFNB1, IFNL1*, *IFNL2*, *MX1*, *CXCL10*, *DDX58*, and other crucial genes for the antiviral response were all downregulated by particle treatments (in hNECs from females), further investigation is necessary to determine whether these changes result in host defense decrements *in vivo*. The SARS-CoV-2-induced interferon response has been shown to be ineffective in controlling viral replication in another study of human airway epithelium (68). While the respiratory epithelium represents the first line of defense to inhaled pollution and pathogens, clearance of infection and inhaled debris relies heavily upon recruitment and activation of immune cells. In our study, particle treatment prior to infection decreased expression of several important chemokines by 72 h p.i. (Tables 5 and 6). It is possible that *in vivo*, the WSP-induced reduction in expression of *CCL3*, *CCL5*, *CXCL10*, *CXCL11*, *CXCL9*, *IL6*, and *TNF*, which are chemoattractants for innate

and adaptive immune cells, would result in a more widespread and lasting infection and delay nasal mucosal antibody production. *In vivo* exposures of mice to diesel exhaust prior to respiratory viral infection increased viral titers and viral mRNA collected from whole lungs (69, 70). Management of viral load mediated by immune cells is not captured in our monoculture model. Finally, many groups have reported effective evasion of interferon and NF-κB pathway activation by SARS-CoV-2 (71-74). Indeed, only a small fraction of infected epithelial cells express the majority of interferons and ISGs (54) suggesting the virus evades or inhibits antiviral responses in most cells it infects. Fig. 3 and Fig. 6 suggest that viral replication and release were underway by 24 h p.i., though ISGs and pro-inflammatory responses were not yet induced by that timepoint. The kinetic delay in cellular responses relative to viral replication as well as antiviral evasion by SARS-CoV-2 likely significantly influence the effects of co-exposure to inhaled pollution on host responses. A longer *in vitro* study which captures the recovery phase after peak antiviral activity (which occurred at our final timepoint, 72 h p.i., in this model) would be informative.

Further work is necessary to elucidate the effects of WSP exposure on SARS-CoV-2 infection, especially in bronchial and small airway epithelial cells and airway macrophages, and with particles derived from other types of biomass or biomass mixtures. Exposure to red oak WSP prior to SARS-CoV-2 infection dampens expression of antiviral and host defense genes in nasal epithelial cells. These effects are sex-dependent, with overall greater downregulation of genes in females than in males. Men have been found to be more susceptible to severe and fatal cases of COVID-19 (17). It is possible that wildfire-derived PM could increase COVID-19 morbidity in exposed females, but additional epidemiological studies are needed. The impact of wildfire smoke on public health in the United States and abroad is expected to increase as wildfire seasons become more intense and the population exposed to wildfire smoke continues to rise (8). As viral pandemics and wildfire exposures continue to be concurrent respiratory health risks it is important to understand their potential synergisms and interactions. This will inform strategies for mitigating risk, especially for subpopulations already susceptible to respiratory infections.

Code Availability

SAS and R codes used for data processing, statistical analysis, and data visualization are provided as a Supplemental File.

Acknowledgments

The authors would like to acknowledge and thank the study coordinators Noelle Knight, Carole Robinette, and Martha Almond for recruiting hNEC donors and retrieving scrape biopsies. The authors would like to thank Shaun McCullough for his generous donation of DEP and Eva Vitucci for her help in making the DEP preparation and determining particle sizes. The authors would also like to thank Yong Ho Kim and Ian Gilmour for their generous contribution of WSP samples. Finally, the authors thank the Advanced Analytics Core for their help and contributions.

Grants

Funding was provided by NIH grants R01 ES031173, T32 ES007126, and P30 DK034987.

Disclosures

The authors have no conflicts of interest to disclose.

References

1. **McClure CD, and Jaffe DA**. US particulate matter air quality improves except in wildfire-prone areas. *Proceedings of the National Academy of Sciences* 115: 7901-7906, 2018.
2. **Jaffe DA, O'Neill SM, Larkin NK, Holder AL, Peterson DL, Halofsky JE, and Rappold AG**. Wildfire and prescribed burning impacts on air quality in the United States. *Journal of the Air & Waste Management Association* 70: 583-615, 2020.
3. **United States, AIRNOW Program**. *AIRNow* [Online]. US Environmental Protection Agency, Office of Air Quality Planning and Standards,. http://www.airnow.gov/. [June, 2021].
4. **Reinhardt T, Ottmar, RD**. Baseline Measurements of Smoke Exposure Among Wildland Firefighters. *Journal of Occupational and Environmental Hygiene* 1: 593-606, 2004.
5. **Reinhardt T, Ottmar, RD**. Smoke Exposure at Western wildfires. *Pacific Northwest Research Station* Res. Pap. PNW-RP-525: 72, 2000.
6. **Swiston JR, Davidson W, Attridge S, Li GT, Brauer M, and Van Eeden SF**. Wood smoke exposure induces a pulmonary and systemic inflammatory response in firefighters. *European Respiratory Journal* 32: 129-138, 2008.
7. **Reid CE, Brauer M, Johnston FH, Jerrett M, Balmes JR, and Elliott CT**. Critical Review of Health Impacts of Wildfire Smoke Exposure. *Environmental Health Perspectives* 124: 1334-1343, 2016.
8. **Reid CE, and Maestas MM**. Wildfire smoke exposure under climate change. *Current Opinion in Pulmonary Medicine* 25: 179-187, 2019.
9. **Fann N, Alman B, Broome RA, Morgan GG, Johnston FH, Pouliot G, and Rappold AG**. The health impacts and economic value of wildland fire episodes in the U.S.: 2008-2012. *Sci Total Environ* 610-611: 802-809, 2018.
10. **Liu JC, Pereira G, Uhl SA, Bravo MA, and Bell ML**. A systematic review of the physical health impacts from non-occupational exposure to wildfire smoke. *Environmental Research* 136: 120-132, 2015.
11. **Kim YH, Warren SH, Krantz QT, King C, Jaskot R, Preston WT, George BJ, Hays MD, Landis MS, Higuchi M, Demarini DM, and Gilmour MI**. Mutagenicity and Lung Toxicity of Smoldering vs. Flaming Emissions from Various Biomass Fuels: Implications for Health Effects from Wildland Fires. *Environmental Health Perspectives* 126: 017011, 2018.

12. **Liu JC, Wilson A, Mickley LJ, Dominici F, Ebisu K, Wang Y, Sulprizio MP, Peng RD, Yue X, Son J-Y, Anderson GB, and Bell ML**. Wildfire-specific Fine Particulate Matter and Risk of Hospital Admissions in Urban and Rural Counties. *Epidemiology* 28: 77-85, 2017.
13. **Reid C, Jerrett, M, Tager, IB, Petersen, ML, Mann, JK, Balmes, JR**. Differential respiratory health effects from the 2008 northern California wildfires: A spatiotemporal approach. *Environmental Research* 150: 227-235, 2016.
14. **World Health Organization**. WHO Coronavirus (COVID-19) Dashboard [Online]. World Health Organization. https://covid19.who.int/. [June 16, 2021].
15. **Finelli L, Gupta V, Petigara T, Yu K, Bauer KA, and Puzniak LA**. Mortality Among US Patients Hospitalized With SARS-CoV-2 Infection in 2020. *JAMA Netw Open* 4: e216556, 2021.
16. **Jin JM, Bai P, He W, Wu F, Liu XF, Han DM, Liu S, and Yang JK**. Gender Differences in Patients With COVID-19: Focus on Severity and Mortality. *Front Public Health* 8: 152, 2020.
17. **Gomez JMD, Du-Fay-De-Lavallaz JM, Fugar S, Sarau A, Simmons JA, Clark B, Sanghani RM, Aggarwal NT, Williams KA, Doukky R, and Volgman AS**. Sex Differences in COVID-19 Hospitalization and Mortality. *Journal of Women's Health* 30: 646-653, 2021.
18. **Centers for Disease Control and Prevention**. Symptoms of COVID-19 [Online]. US Dept of Health and Human Services. https://www.cdc.gov/coronavirus/2019-ncov/symptoms-testing/symptoms.html. [June, 18, 2021].
19. **Hou YJ, Okuda K, Edwards CE, Martinez DR, Asakura T, Dinnon KH, 3rd, Kato T, Lee RE, Yount BL, Mascenik TM, Chen G, Olivier KN, Ghio A, Tse LV, Leist SR, Gralinski LE, Schäfer A, Dang H, Gilmore R, Nakano S, Sun L, Fulcher ML, Livraghi-Butrico A, Nicely NI, Cameron M, Cameron C, Kelvin DJ, de Silva A, Margolis DM, Markmann A, Bartelt L, Zumwalt R, Martinez FJ, Salvatore SP, Borczuk A, Tata PR, Sontake V, Kimple A, Jaspers I, O'Neal WK, Randell SH, Boucher RC, and Baric RS**. SARS-CoV-2 Reverse Genetics Reveals a Variable Infection Gradient in the Respiratory Tract. *Cell* 182: 429-446.e414, 2020.
20. **Lee MK, Yoo JW, Lin H, Kim YS, Kim DD, Choi YM, Park SK, Lee CH, and Roh HJ**. Air-liquid interface culture of serially passaged human nasal epithelial cell monolayer for in vitro drug transport studies. *Drug Deliv* 12: 305-311, 2005.
21. **Müller L, Brighton LE, Carson JL, Fischer WA, and Jaspers I**. Culturing of Human Nasal Epithelial Cells at the Air Liquid Interface. *Journal of Visualized Experiments* 2013.
22. **Sungnak W, Huang N, Bécavin C, Berg M, Queen R, Litvinukova M, Talavera-López C, Maatz H, Reichart D, Sampaziotis F, Worlock KB, Yoshida M, and Barnes JL**. SARS-CoV-2 entry factors are highly expressed in nasal epithelial cells together with innate immune genes. *Nature Medicine* 26: 681-687, 2020.
23. **Jaspers I, Ciencewicki, JM, Zhang, W, Brighton, LE, Carson, JL, Beck, MA, Madden, MC**. Diesel Exhaust enhances influenza virus infections in respiratory epithelial cells. *Toxicological Sciences* 85: 990-1002, 2005.
24. **Spannhake EW, Reddy SP, Jacoby DB, Yu XY, Saatian B, and Tian J**. Synergism between rhinovirus infection and oxidant pollutant exposure enhances airway epithelial cell cytokine production. *Environ Health Perspect* 110: 665-670, 2002.
25. **Clapp PW, Lavrich KS, Van Heusden CA, Lazarowski ER, Carson JL, and Jaspers I**. Cinnamaldehyde in flavored e-cigarette liquids temporarily suppresses bronchial epithelial cell ciliary motility by dysregulation of mitochondrial function. *American Journal of Physiology-Lung Cellular and Molecular Physiology* 316: L470-L486, 2019.
26. **Escobar Y-NH, Morrison CB, Chen Y, Hickman E, Love CA, Rebuli ME, Surratt JD, Ehre C, and Jaspers I**. Differential responses to e-cig generated aerosols from humectants and different forms of nicotine in epithelial cells from non-smokers and smokers. *American Journal of Physiology-Lung Cellular and Molecular Physiology* 0: null.
27. **Kesic MJ, Meyer M, Bauer R, and Jaspers I**. Exposure to ozone modulates human airway protease/antiprotease balance contributing to increased influenza A infection. *PLoS One* 7: e35108, 2012.
28. **Ciencewicki J, and Jaspers I**. Air pollution and respiratory viral infection. *Inhal Toxicol* 19: 1135-1146, 2007.
29. **Rebuli ME, Brocke SA, and Jaspers I**. Impact of Inhaled Pollutants on Response to Viral Infection in Controlled Exposures. *Journal of Allergy and Clinical Immunology* 2021.
30. **Rebuli ME, Speen AM, Martin EM, Addo KA, Pawlak EA, Glista-Baker E, Robinette C, Zhou H, Noah TL, and Jaspers I**. Wood Smoke Exposure Alters Human Inflammatory Responses to Viral Infection in a Sex-Specific Manner. A Randomized, Placebo-controlled Study. *American Journal of Respiratory and Critical Care Medicine* 199: 996-1007, 2019.
31. **Wu X, Nethery RC, Sabath MB, Braun D, and Dominici F**. Air pollution and COVID-19 mortality in the United States: Strengths and limitations of an ecological regression analysis. *Science Advances* 6: eabd4049, 2020.
32. **Travaglio M, Yu Y, Popovic R, Selley L, Leal NS, and Martins LM**. Links between air pollution and COVID-19 in England. *Environmental Pollution* 268: 115859, 2021.

33. **Liang D, Shi L, Zhao J, Liu P, Sarnat JA, Gao S, Schwartz J, Liu Y, Ebelt ST, Scovronick N, and Chang HH**. Urban Air Pollution May Enhance COVID-19 Case-Fatality and Mortality Rates in the United States. *The Innovation* 1: 100047, 2020.
34. **Stieb DM, Evans GJ, To TM, Brook JR, and Burnett RT**. An ecological analysis of long-term exposure to PM2.5 and incidence of COVID-19 in Canadian health regions. *Environmental Research* 191: 110052, 2020.
35. **Cole M, Ozgen, C, Strobl, E**. Air Pollution Exposure and COVID-19. *IZA Institute of Labor Economics* DP No. 13367: 2020.
36. **Zhou X, Josey K, Kamareddine L, Caine MC, Liu T, Mickley LJ, Cooper M, and Dominici F**. Excess of COVID-19 cases and deaths due to fine particulate matter exposure during the 2020 wildfires in the United States. *Science Advances* 7: eabi8789, 2021.
37. **Kiser D, Elhanan G, Metcalf WJ, Schnieder B, and Grzymski JJ**. SARS-CoV-2 test positivity rate in Reno, Nevada: association with PM2.5 during the 2020 wildfire smoke events in the western United States. *Journal of Exposure Science & Environmental Epidemiology* 2021.
38. **Sagai M, Saito, H., Ichinose, T., Kodama, M., Mori, Y.** Biological Effects of Diesel Exhaust Particles. I. In Vitro Production of Superoxide and In Vivo Toxicity in Mouse. *Free Radical Biology and Medicine* 14: 37-47, 1993.
39. **Zhu Y, Xie J, Huang F, and Cao L**. Association between short-term exposure to air pollution and COVID-19 infection: Evidence from China. *Science of The Total Environment* 727: 138704, 2020.
40. **Wang B, Liu J, Li Y, Fu S, Xu X, Li L, Zhou J, Liu X, He X, Yan J, Shi Y, Niu J, Yang Y, Li Y, Luo B, and Zhang K**. Airborne particulate matter, population mobility and COVID-19: a multi-city study in China. *BMC Public Health* 20: 2020.
41. **Muala A, Rankin G, Sehlstedt M, Unosson J, Bosson JA, Behndig A, Pourazar J, Nyström R, Pettersson E, Bergvall C, Westerholm R, Jalava PI, Happo MS, Uski O, Hirvonen M-R, Kelly FJ, Mudway IS, Blomberg A, Boman C, and Sandström T**. Acute exposure to wood smoke from incomplete combustion - indications of cytotoxicity. *Particle and Fibre Toxicology* 12: 2015.
42. **Sehlstedt M, Dove R, Boman C, Pagels J, Swietlicki E, Löndahl J, Westerholm R, Bosson J, Barath S, Behndig AF, Pourazar J, Sandström T, Mudway IS, and Blomberg A**. Antioxidant airway responses following experimental exposure to wood smoke in man. *Particle and Fibre Toxicology* 7: 21, 2010.
43. **Stockfelt L, Sallsten G, Almerud P, Basu S, and Barregard L**. Short-term chamber exposure to low doses of two kinds of wood smoke does not induce systemic inflammation, coagulation or oxidative stress in healthy humans. *Inhalation Toxicology* 25: 417-425, 2013.
44. **Hansson A, Rankin G, Uski O, Sehlstedt M, Bosson J, Pourazar J, Boman C, Lindgren R, Garcia Lopez N, Behndig A, Blomberg A, Sandström T, and Muala A**. Wood smoke effects on epithelial cell lines and human airway cells. *European Respiratory Journal* 54: PA5448, 2019.
45. **Dilger M, Orasche J, Zimmermann R, Paur H-R, Diabaté S, and Weiss C**. Toxicity of wood smoke particles in human A549 lung epithelial cells: the role of PAHs, soot and zinc. *Archives of Toxicology* 90: 3029-3044, 2016.
46. **Danielsen PH, Møller P, Jensen KA, Sharma AK, Wallin HK, Bossi R, Autrup H, Mølhave L, Ravanat J-L, Briedé JJ, De Kok TM, and Loft S**. Oxidative Stress, DNA Damage, and Inflammation Induced by Ambient Air and Wood Smoke Particulate Matter in Human A549 and THP-1 Cell Lines. *Chemical Research in Toxicology* 24: 168-184, 2011.
47. **Roscioli E, Hamon R, Lester SE, Jersmann HPA, Reynolds PN, and Hodge S**. Airway epithelial cells exposed to wildfire smoke extract exhibit dysregulated autophagy and barrier dysfunction consistent with COPD. *Respiratory Research* 19: 2018.
48. **Holder AL, Lucas D, Goth-Goldstein R, and Koshland CP**. Cellular Response to Diesel Exhaust Particles Strongly Depends on the Exposure Method. *Toxicological Sciences* 103: 108-115, 2008.
49. **Sager TM, and Castranova V**. Surface area of particle administered versus mass in determining the pulmonary toxicity of ultrafine and fine carbon black: comparison to ultrafine titanium dioxide. *Particle and Fibre Toxicology* 6: 15, 2009.
50. **Lison D, Lardot C, X000E, Cile, Huaux F, X000E, Ois, Zanetti G, and Fubini B**. Influence of particle surface area on the toxicity of insoluble manganese dioxide dusts. *Archives of Toxicology* 71: 725-729, 1997.
51. **Tyler CR, Zychowski KE, Sanchez BN, Rivero V, Lucas S, Herbert G, Liu J, Irshad H, McDonald JD, Bleske BE, and Campen MJ**. Surface area-dependence of gas-particle interactions influences pulmonary and neuroinflammatory outcomes. *Particle and Fibre Toxicology* 13: 2016.
52. **Heyder J, Gebhart J, Rudolf G, Schiller CF, and Stahlhofen W**. Deposition of particles in the human respiratory tract in the size range 0.005–15 μm. *Journal of Aerosol Science* 17: 811-825, 1986.
53. **Rager J, Clark, J, Eaves, LA, Avula, V, Niehoff, NM, Kim, YH, Jaspers, I, Gilmour, MI**. Mixtures modeling identifies chemical inducers versus repressors of toxicity associated with wildfire smoke. *Sci Total Environ* 775: 2021.

54. **Fiege JK, Thiede JM, Nanda HA, Matchett WE, Moore PJ, Montanari NR, Thielen BK, Daniel J, Stanley E, Hunter RC, Menachery VD, Shen SS, Bold TD, and Langlois RA**. Single cell resolution of SARS-CoV-2 tropism, antiviral responses, and susceptibility to therapies in primary human airway epithelium. *PLOS Pathogens* 17: e1009292, 2021.
55. **Lieberman NAP, Peddu V, Xie H, Shrestha L, Huang M-L, Mears MC, Cajimat MN, Bente DA, Shi P-Y, Bovier F, Roychoudhury P, Jerome KR, Moscona A, Porotto M, and Greninger AL**. In vivo antiviral host transcriptional response to SARS-CoV-2 by viral load, sex, and age. *PLOS Biology* 18: e3000849, 2020.
56. **Kim Y-M, and Shin E-C**. Type I and III interferon responses in SARS-CoV-2 infection. *Experimental & Molecular Medicine* 53: 750-760, 2021.
57. **Park A, and Iwasaki A**. Type I and Type III Interferons – Induction, Signaling, Evasion, and Application to Combat COVID-19. *Cell Host & Microbe* 27: 870-878, 2020.
58. **Ziegler CGK, Allon SJ, Nyquist SK, Mbano IM, Miao VN, Tzouanas CN, Cao Y, Yousif AS, Bals J, Hauser BM, Feldman J, Muus C, Wadsworth MH, 2nd, Kazer SW, Hughes TK, Doran B, Gatter GJ, Vukovic M, Taliaferro F, Mead BE, Guo Z, Wang JP, Gras D, Plaisant M, Ansari M, Angelidis I, Adler H, Sucre JMS, Taylor CJ, Lin B, Waghray A, Mitsialis V, Dwyer DF, Buchheit KM, Boyce JA, Barrett NA, Laidlaw TM, Carroll SL, Colonna L, Tkachev V, Peterson CW, Yu A, Zheng HB, Gideon HP, Winchell CG, Lin PL, Bingle CD, Snapper SB, Kropski JA, Theis FJ, Schiller HB, Zaragosi LE, Barbry P, Leslie A, Kiem HP, Flynn JL, Fortune SM, Berger B, Finberg RW, Kean LS, Garber M, Schmidt AG, Lingwood D, Shalek AK, and Ordovas-Montanes J**. SARS-CoV-2 Receptor ACE2 Is an Interferon-Stimulated Gene in Human Airway Epithelial Cells and Is Detected in Specific Cell Subsets across Tissues. *Cell* 181: 1016-1035.e1019, 2020.
59. **Schoggins J, Rice, CM**. Interferon-stimulated genes and their antiviral effector functions. *Curr Opin Virol* 1: 519-525, 2011.
60. **Patra T, Meyer K, Geerling L, Isbell TS, Hoft DF, Brien J, Pinto AK, Ray RB, and Ray R**. SARS-CoV-2 spike protein promotes IL-6 trans-signaling by activation of angiotensin II receptor signaling in epithelial cells. *PLOS Pathogens* 16: e1009128, 2020.
61. **Schroeder S, Pott F, Niemeyer D, Veith T, Richter A, Muth D, Goffinet C, Müller MA, and Drosten C**. Interferon antagonism by SARS-CoV-2: a functional study using reverse genetics. *The Lancet Microbe* 2: e210-e218, 2021.
62. **Hemmat N, Asadzadeh Z, Ahangar NK, Alemohammad H, Najafzadeh B, Derakhshani A, Baghbanzadeh A, Baghi HB, Javadrashid D, Najafi S, Ar Gouilh M, and Baradaran B**. The roles of signaling pathways in SARS-CoV-2 infection; lessons learned from SARS-CoV and MERS-CoV. *Archives of Virology* 166: 675-696, 2021.
63. **Hirano T, and Murakami M**. COVID-19: A New Virus, but a Familiar Receptor and Cytokine Release Syndrome. *Immunity* 52: 731-733, 2020.
64. **Hariharan A, Hakeem AR, Radhakrishnan S, Reddy MS, and Rela M**. The Role and Therapeutic Potential of NF-kappa-B Pathway in Severe COVID-19 Patients. *Inflammopharmacology* 29: 91-100, 2021.
65. **Majumdar S, and Murphy PM**. Chemokine Regulation During Epidemic Coronavirus Infection. *Front Pharmacol* 11: 600369-600369, 2021.
66. **Stapleton EM, Welch JL, Ubeda EA, Xiang J, Zabner J, Thornell IM, Nonnenmann MW, Stapleton JT, and Comellas AP**. Urban particulate matter impairs airway-surface-liquid-mediated coronavirus inactivation. *The Journal of Infectious Diseases* 2021.
67. **Hoffmann M, Kleine-Weber H, Schroeder S, Krüger N, Herrler T, Erichsen S, Schiergens TS, Herrler G, Wu N-H, Nitsche A, Müller MA, Drosten C, and Pöhlmann S**. SARS-CoV-2 Cell Entry Depends on ACE2 and TMPRSS2 and Is Blocked by a Clinically Proven Protease Inhibitor. *Cell* 181: 271-280.e278, 2020.
68. **Rebendenne A, Valadao ALC, Tauziet M, Maarifi G, Bonaventure B, McKellar J, Planes R, Nisole S, Arnaud-Arnould M, Moncorge O, and Goujon C**. SARS-CoV-2 Triggers an MDA-5-Dependent Interferon Response Which is Unable to Control Replication in Lung Epithelial Cells. *Journal of Virology* 95: 2021.
69. **Harrod K, Jaramillo, RJ, Rosenberger, CL, Wang, SZ, Berger, JA, McDonald, JD, Reed, MD**. Increased susceptibility to RSV infection by exposure to inhaled diesel engine emissions. *Am J Respir Cell Mol Biol* 28: 451-463, 2003.
70. **Gowdy K, Krantz, QT, King, C, Boykin E, Jaspers, I, Linak, WP, Gilmour, MI**. Role of oxidative stress on diesel-enhanced influenza infection in mice. *Particle and Fibre Toxicology* 7: 1-15, 2010.
71. **Xia H, Cao Z, Xie X, Zhang X, Chen JY-C, Wang H, Menachery VD, Rajsbaum R, and Shi P-Y**. Evasion of Type I Interferon by SARS-CoV-2. *Cell reports* 33: 108234-108234, 2020.
72. **Lei X, Dong X, Ma R, Wang W, Xiao X, Tian Z, Wang C, Wang Y, Li L, Ren L, Guo F, Zhao Z, Zhou Z, Xiang Z, and Wang J**. Activation and evasion of type I interferon responses by SARS-CoV-2. *Nature Communications* 11: 3810, 2020.

73. **Hayn M, Hirschenberger M, Koepke L, Nchioua R, Straub JH, Klute S, Hunszinger V, Zech F, Prelli Bozzo C, Aftab W, Christensen MH, Conzelmann C, Müller JA, Srinivasachar Badarinarayan S, Stürzel CM, Forne I, Stenger S, Conzelmann K-K, Münch J, Schmidt FI, Sauter D, Imhof A, Kirchhoff F, and Sparrer KMJ**. Systematic functional analysis of SARS-CoV-2 proteins uncovers viral innate immune antagonists and remaining vulnerabilities. *Cell Reports* 35: 109126, 2021.

74. **Vazquez C, Swanson SE, Negatu SG, Dittmar M, Miller J, Ramage HR, Cherry S, and Jurado KA**. SARS-CoV-2 viral proteins NSP1 and NSP13 inhibit interferon activation through distinct mechanisms. *PLOS ONE* 16: e0253089, 2021.

Figure Legends:

Fig. 1: Experimental design scheme. Differentiated hNECs from males and females grown at ALI were exposed to 22 μg/cm^2 DEP, eucalyptus WSP, or red oak WSP (or control) for 2 h. At the end of the exposure period, cells were infected with SARS-CoV-2 at an M.O.I. of 0.5 (or mock infected with vehicle) for 2 h. Excess virus and residual particles were then removed and the apical surface was washed. A second apical wash and cell lysis were performed immediately or 24 or 72 h later. Apical washes were used to determine viral titers and RNA was purified from cell lysates and used for RT-qPCR to assess altered gene expression in a panel of 48 genes. Figure created with BioRender.com.

Fig. 2: Effects of particle exposure on gene expression (-ΔΔCt) in uninfected hNECs at 0, 24, and 72 h post (mock) infection. Corresponds to 2, 26, and 74 h post exposure to particles. Gene categories are color-coded at the top, with 'VEF' an abbreviation for 'Viral Entry Factor' and 'Surf.' an abbreviation for 'Surfactant'. Graphed as means with black bars representing standard error. Males and females are combined (N=6 biological replicates for each bar). Statistically significant changes in gene expression are denoted by * ($q \leq 0.05$).

Fig. 3: Gene expression in infected hNECs from males and females relative to uninfected controls at 0, 24, and 72 h p.i. Graphed as average (N=9 biological replicates for each bar) with standard error. Statistically significant ($q \leq 0.05$) changes in gene expression are represented by *. A statistically significant difference in gene expression between males and females is indicated by #.

Fig. 4: Effects of particle exposure (DEP and WSP) on virus-induced gene expression in infected hNECs at 72 h p.i. Graphed as means with black bars representing standard error. Males and females are combined for N=6 biological replicates per bar. Statistically significant changes in gene expression are indicated by * ($q \leq 0.05$).

Fig. 5: Effects of particle exposure on virus-induced gene expression in infected hNECs from males or females at 72 h post infection. Graphed as means with black bars representing standard error, N=3 biological replicates per bar. Statistically significant changes in gene expression are represented by * and statistically significant differences in expression between males and females are represented by # ($q \leq 0.05$).

Fig. 6: SARS-CoV-2 viral titers in hNEC cultures at 0, 24, and 72 h p.i. hNECs from male and female donors were exposed to particles (DEP or WSP from flaming eucalyptus or red oak, at 22 μg/cm^2) or control for 2 h, then infected with SARS-CoV-2 at an MOI of 0.5. At 0, 24, or 72 h post infection, the apical washes were collected and used for approximating viral titer. Titers from individual particle exposures with respective controls for DEP, eucalyptus WSP, and red oak WSP are shown in **A-C** respectively. Black symbols indicate sex-specific means with standard error bars (N=3 biological replicates each for males and females). **D** Aggregated viral titers recovered from hNECs exposed to vehicle or a particle. Standard error is shown (N=9 biological replicates for each bar). Unpaired t-tests with Welch's correction were used to determine (sex aggregated) differences in viral titer between time points, with *** $p = 0.0001$, **** $p < 0.0001$.

Fig. 7: Relationship between gene expression relative to reference genes (-ΔCt) and $\log_{10}$(viral titer) in infected cells. Colors behind gene names correspond to functional categories presented in Table 2. Statistical significance is indicated next to the coefficient of determination (R^2): * $p \leq 0.05$, ** $p \leq 0.01$, *** $p \leq 0.001$.

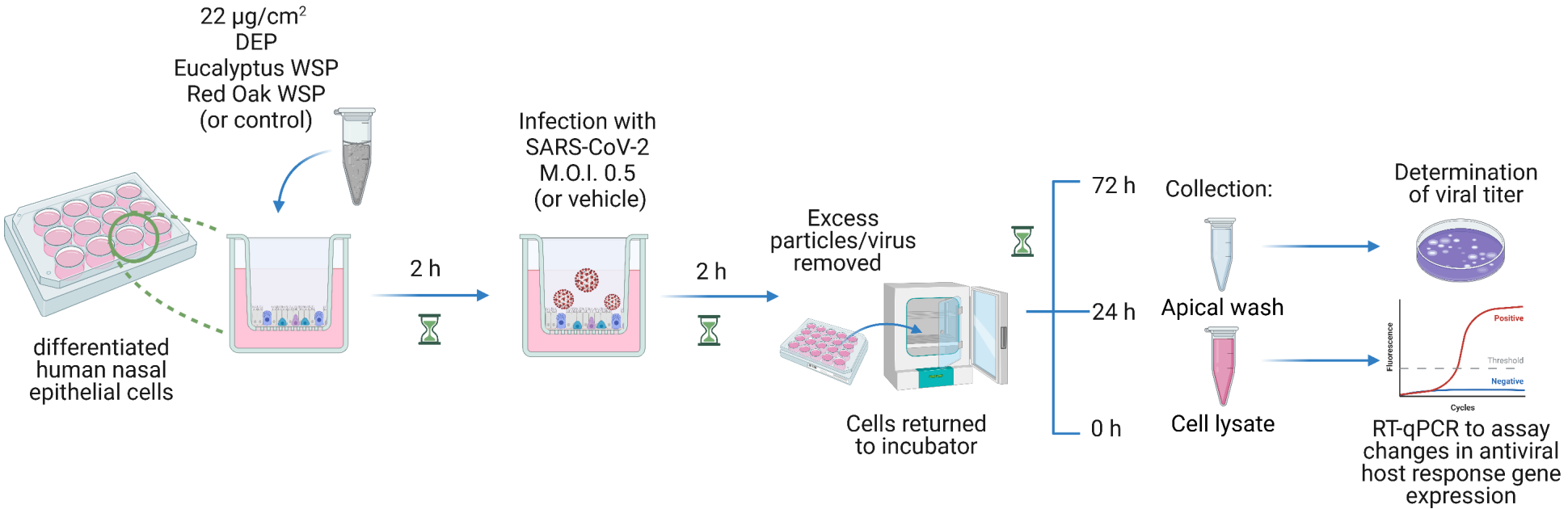
22 µg/cm²
DEP
Eucalyptus WSP
Red Oak WSP
(or control)
differentiated
human nasal
epithelial cells
2 h
Infection with
SARS-CoV-2
M.O.I. 0.5
(or vehicle)
2 h
Excess
particles/virus
removed
Cells returned
to incubator
72 h
24 h
0 h
Collection:
Apical wash
Cell lysate
Determination
of viral titer
Positive
Threshold
Negative
Fluorescence
Cycles
RT-qPCR to assay
changes in antiviral
host response gene
expression


VEF
Airway Proteases
Antiviral Defense
Cell Signaling/Immune Cell Recruitment
Mucins
Surf.
Transcription Factors
Viral Recognition
Gene Expression Relative to Untreated Controls, Normalized to Reference Genes (-ΔΔCt)
2.5
0.0
-2.5
-5.0
0h
24h
72h
Particle Exposure
Diesel Exhaust
Eucalyptus Wood Smoke
Red Oak Wood Smoke
ACE2
CTSB
CTSL
FURIN
MMP7
ST14
TMPRSS11D
TMPRSS2
IFIT1
IFITM3
IFNA1
IFNA2
IFNB1
IFNG
IFNL1
IFNL2
LTF
MX1
SOCS3
CCL2
CCL3
CCL5
CSF2
CXCL10
CXCL11
CXCL8
CXCL9
IL15
IL1B
IL6
TNF
MUC5AC
MUC5B
SFTPA1
SFTPD
IRF1
IRF3
IRF7
NFKB1
STAT1
STAT2
STAT3
DDX58
TLR3
TLR7
TLR9
Gene

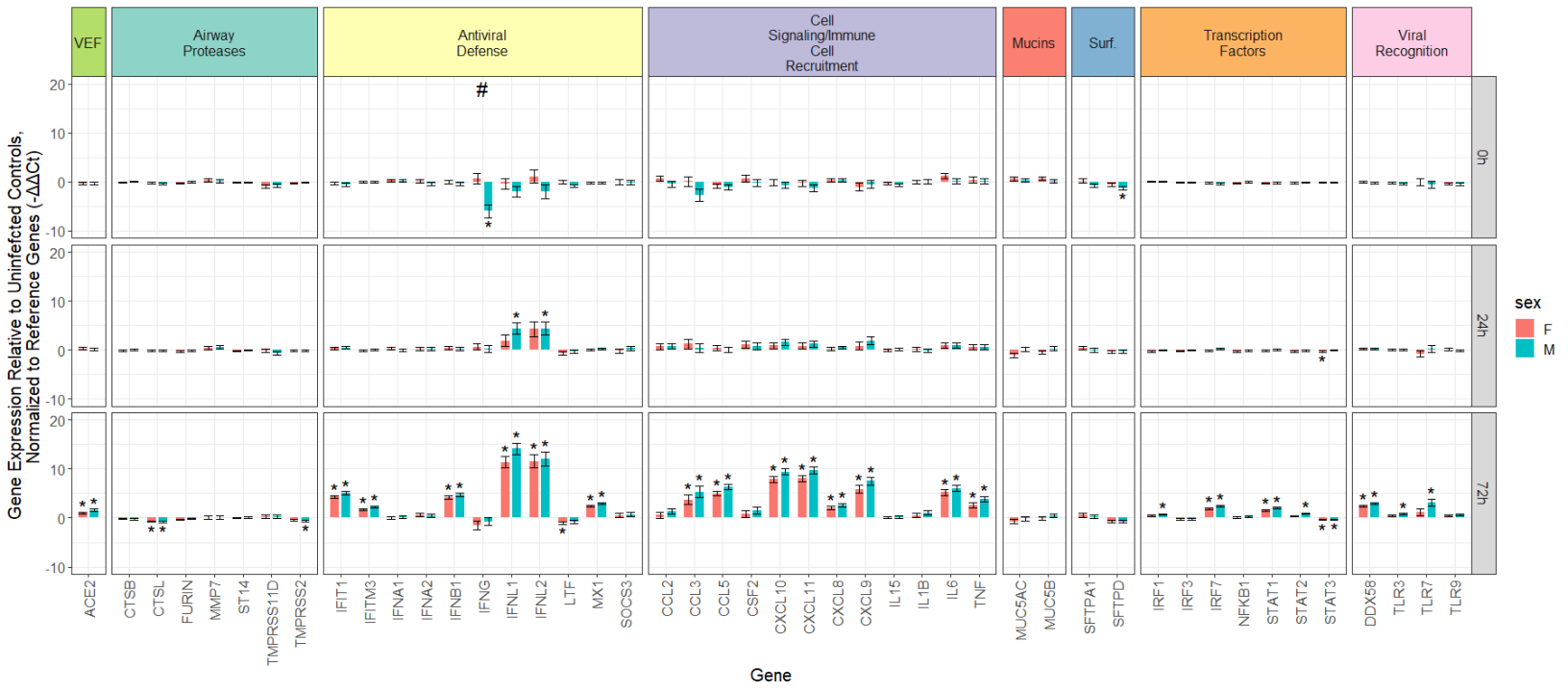
VEF
Airway Proteases
Antiviral Defense
Cell Signaling/Immune Cell Recruitment
Mucins
Surf.
Transcription Factors
Viral Recognition
0h
24h
72h
sex
F
M
Gene Expression Relative to Uninfected Controls, Normalized to Reference Genes (-ΔΔCt)
Gene
ACE2
CTSB
CTSL
FURIN
MMP7
ST14
TMPRSS11D
TMPRSS2
IFIT1
IFITM3
IFNA1
IFNA2
IFNB1
IFNG
IFNL1
IFNL2
LTF
MX1
SOCS3
CCL2
CCL3
CCL5
CSF2
CXCL10
CXCL11
CXCL8
CXCL9
IL15
IL1B
IL6
TNF
MUC5AC
MUC5B
SFTPA1
SFTPD
IRF1
IRF3
IRF7
NFKB1
STAT1
STAT2
STAT3
DDX58
TLR3
TLR7
TLR9

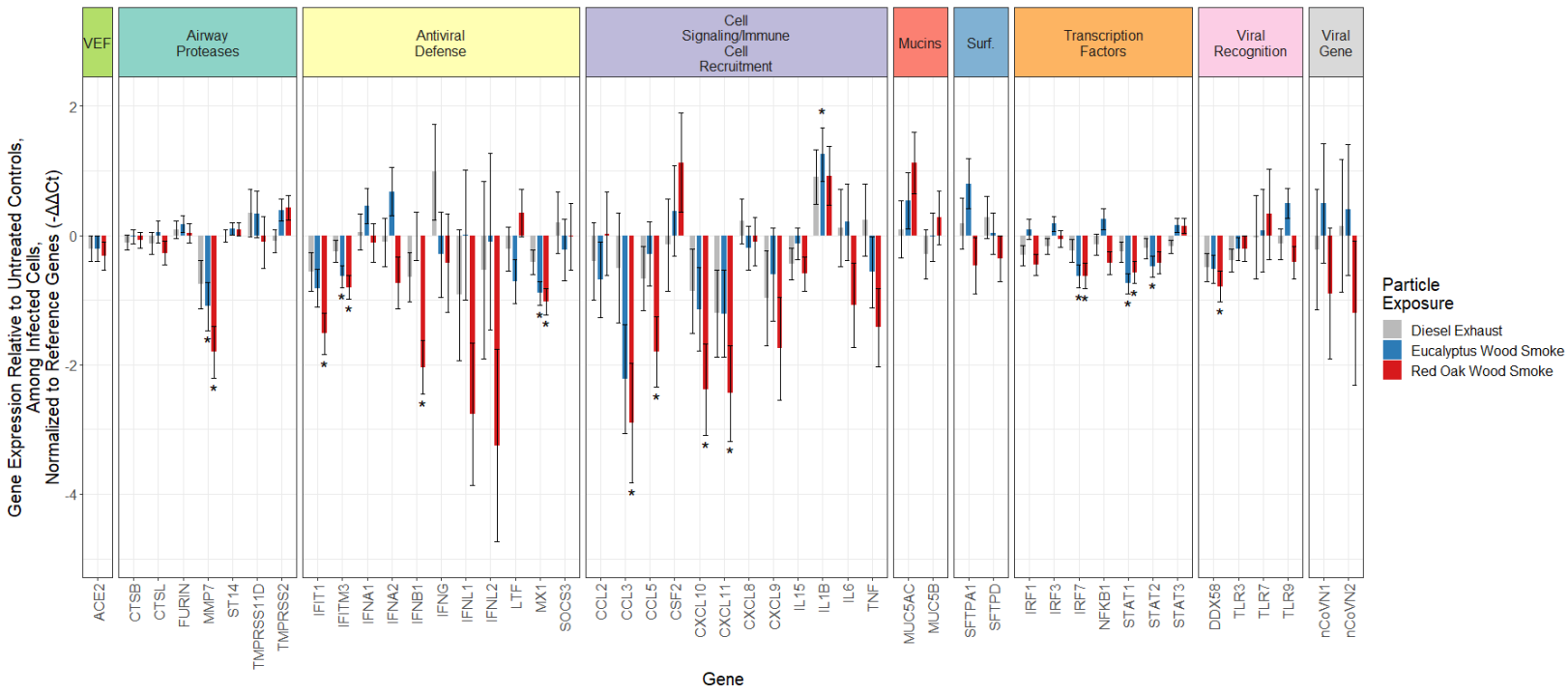
VEF
Airway Proteases
Antiviral Defense
Cell Signaling/Immune Cell Recruitment
Mucins
Surf.
Transcription Factors
Viral Recognition
Viral Gene
Gene Expression Relative to Untreated Controls, Among Infected Cells, Normalized to Reference Genes (-ΔΔCt)
2
0
-2
-4
ACE2
CTSB
CTSL
FURIN
MMP7
ST14
TMPRSS11D
TMPRSS2
IFIT1
IFITM3
IFNA1
IFNA2
IFNB1
IFNG
IFNL1
IFNL2
LTF
MX1
SOCS3
CCL2
CCL3
CCL5
CSF2
CXCL10
CXCL11
CXCL8
CXCL9
IL15
IL1B
IL6
TNF
MUC5AC
MUC5B
SFTPA1
SFTPD
IRF1
IRF3
IRF7
NFKB1
STAT1
STAT2
STAT3
DDX58
TLR3
TLR7
TLR9
nCoVN1
nCoVN2
Gene
Particle Exposure
Diesel Exhaust
Eucalyptus Wood Smoke
Red Oak Wood Smoke

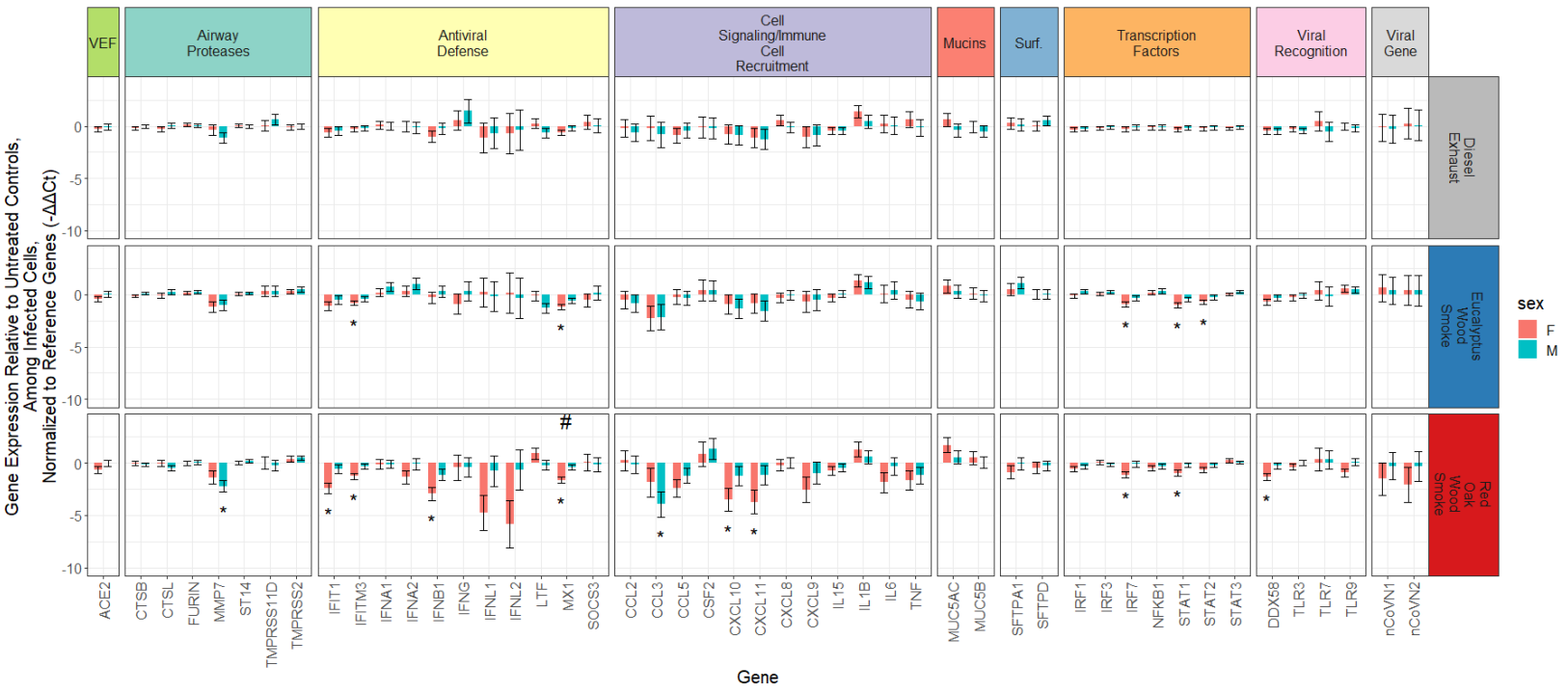
VEF
Airway Proteases
Antiviral Defense
Cell Signaling/Immune Cell Recruitment
Mucins
Surf.
Transcription Factors
Viral Recognition
Viral Gene
Diesel Exhaust
Eucalyptus Wood Smoke
Red Oak Wood Smoke
Gene Expression Relative to Untreated Controls, Among Infected Cells, Normalized to Reference Genes (-ΔΔCt)
0
-5
-10
ACE2
CTSB
CTSL
FURIN
MMP7
ST14
TMPRSS11D
TMPRSS2
IFIT1
IFITM3
IFNA1
IFNA2
IFNB1
IFNG
IFNL1
IFNL2
LTF
MX1
SOCS3
CCL2
CCL3
CCL5
CSF2
CXCL10
CXCL11
CXCL8
CXCL9
IL15
IL1B
IL6
TNF
MUC5AC
MUC5B
SFTPA1
SFTPD
IRF1
IRF3
IRF7
NFKB1
STAT1
STAT2
STAT3
DDX58
TLR3
TLR7
TLR9
nCoVN1
nCoVN2
Gene
sex
F
M

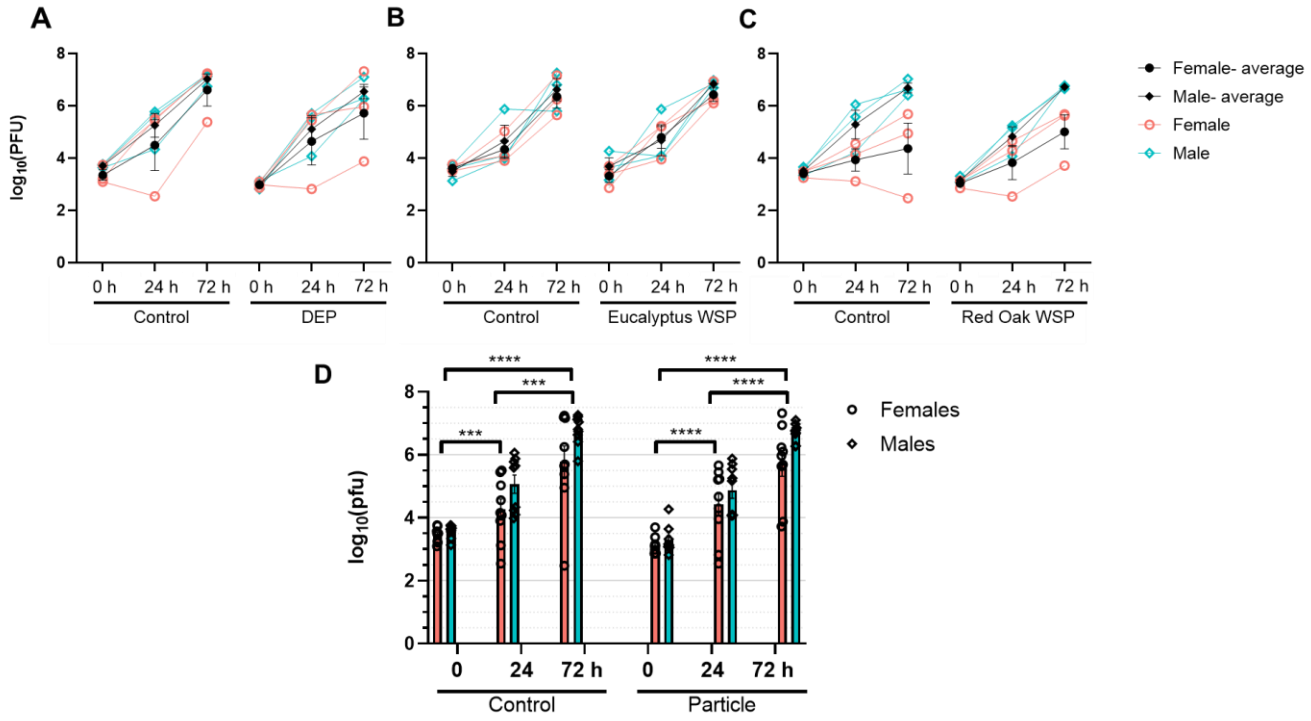
A
B
C
log10(PFU)
0 h
24 h
72 h
Control
DEP
Eucalyptus WSP
Red Oak WSP
Female- average
Male- average
Female
Male
D
log10(pfu)
****
***
Females
Males
Particle

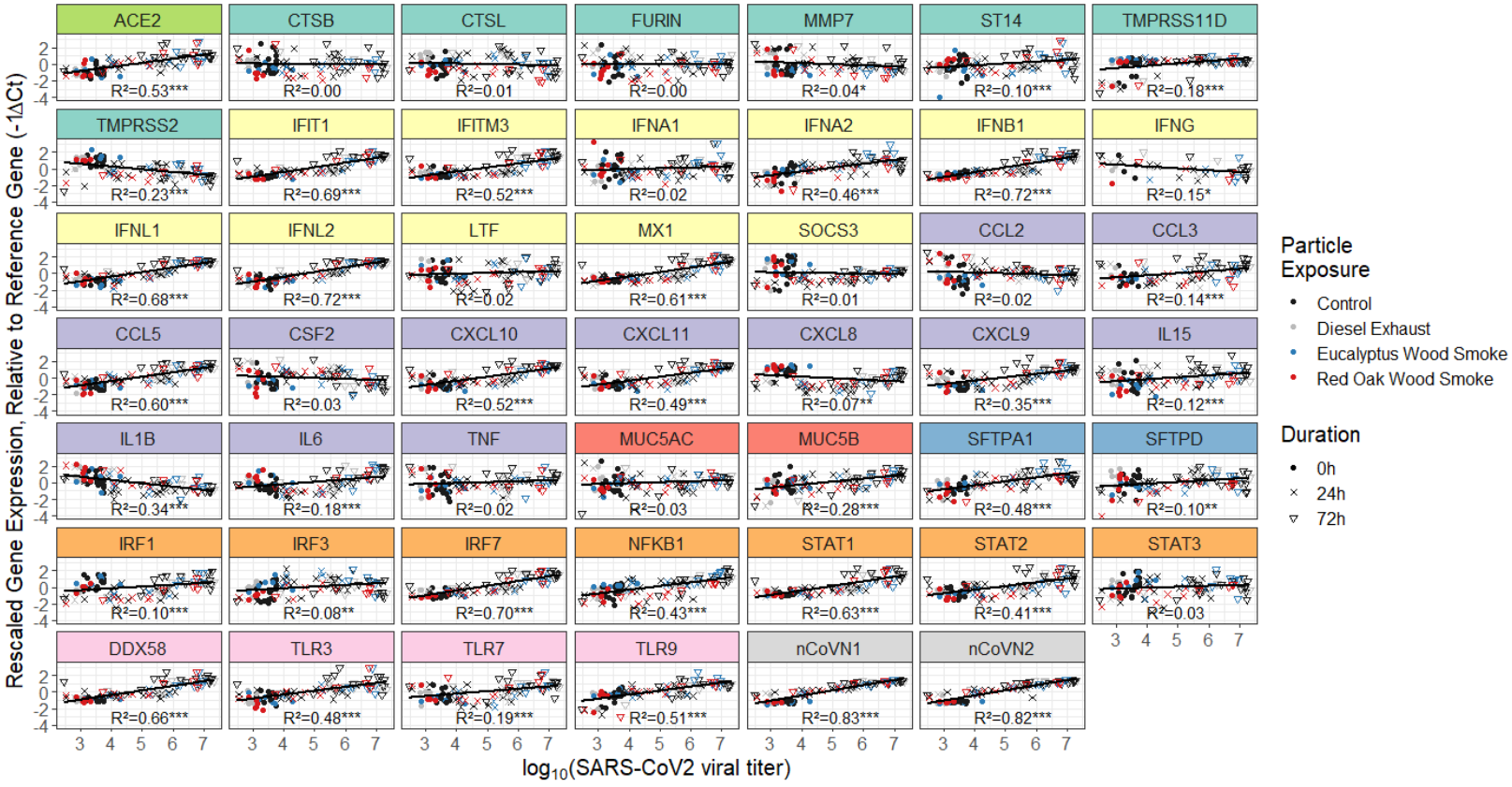
ACE2 R²=0.53***
CTSB R²=0.00
CTSL R²=0.01
FURIN R²=0.00
MMP7 R²=0.04*
ST14 R²=0.10***
TMPRSS11D R²=0.18***
TMPRSS2 R²=0.23***
IFIT1 R²=0.69***
IFITM3 R²=0.52***
IFNA1 R²=0.02
IFNA2 R²=0.46***
IFNB1 R²=0.72***
IFNG R²=0.15*
IFNL1 R²=0.68***
IFNL2 R²=0.72***
LTF R²=0.02
MX1 R²=0.61***
SOCS3 R²=0.01
CCL2 R²=0.02
CCL3 R²=0.14***
CCL5 R²=0.60***
CSF2 R²=0.03
CXCL10 R²=0.52***
CXCL11 R²=0.49***
CXCL8 R²=0.07**
CXCL9 R²=0.35***
IL15 R²=0.12***
IL1B R²=0.34***
IL6 R²=0.18***
TNF R²=0.02
MUC5AC R²=0.03
MUC5B R²=0.28***
SFTPA1 R²=0.48***
SFTPD R²=0.10**
IRF1 R²=0.10***
IRF3 R²=0.08**
IRF7 R²=0.70***
NFKB1 R²=0.43***
STAT1 R²=0.63***
STAT2 R²=0.41***
STAT3 R²=0.03
DDX58 R²=0.66***
TLR3 R²=0.48***
TLR7 R²=0.19***
TLR9 R²=0.51***
nCoVN1 R²=0.83***
nCoVN2 R²=0.82***
Rescaled Gene Expression, Relative to Reference Gene (-1ΔCt)
log10(SARS-CoV2 viral titer)
Particle Exposure
Control
Diesel Exhaust
Eucalyptus Wood Smoke
Red Oak Wood Smoke
Duration
0h
24h
72h

Table 1: Demographic information about hNEC donors

	DEP (n=6)			Eucalyptus WSP (n=6)			Red Oak WSP (n=6)		
	Males (n=3)	Females (n=3)	**Aggregate (Males and Females)**	Males (n=3)	Females (n=3)	**Aggregate (Males and Females)**	Males (n=3)	Females (n=3)	**Aggregate (Males and Females)**
Age (mean ± SEM)	32±5.7	33.0±6.1	**32.5±3.7**	23.7±2.9	23.3±2.8	**23.5±1.8**	20.7±1.2	29.3±5.0	**25.0±3.0**
BMI (mean ± SEM)	27.8±3.1	26.5±1.4	**27.1±1.6**	23.5±0.8	29.9±6.1	**26.7±3.1**	24.3±1.5	26.9±3.8	**25.6±1.9**
Race: White/Black/Asian	2/1/0	3/0/0	**5/1/0**	1/0/2	2/1/0	**3/1/2**	0/0/3	1/1/1	**1/1/4**

Table 2: Genes assayed, grouped by functional categories. Assay identifiers are listed for TaqMan primer/probe sets purchased from Thermo Fisher (or IDT where indicated).

Functional Category:	Gene Name:	Encoded Protein:	TaqMan Probe Assay ID:
Viral Entry Factor (VEF)	*ACE2*	Angiotensin converting enzyme 2	Hs01085331_m1
Airway Proteases	*CTSB*	Cathepsin B	Hs00157194_m1
	CTSL	Cathepsin L	Hs00964651_m1
	FURIN	Furin	Hs06637404_sH
	MMP7	Matrix metallopeptidase 7	Hs01042796_m1
	ST14	ST14 transmembrane serine protease matriptase	Hs01058386_m1
	TMPRSS11D	Transmembrane serine protease 11D	Hs00975370_m1
	TMPRSS2	Transmembrane serine protease 2	Hs05024838_m1
Antiviral Defense	*IFIT1*	Interferon induced protein with tetratricopeptide repeats 1	Hs03027069_s1
	IFITM3	Interferon induced transmembrane protein 3	Hs03057129_s1
	IFNA1	Interferon alpha 1	Hs04189288_g1
	IFNA2	Interferon alpha 2	Hs00265051_s1
	IFNB1	Interferon beta 1	Hs00265051_s2
	IFNG	Interferon gamma	Hs00265051_s3
	IFNL1	Interferon lambda 1	Hs00265051_s4
	IFNL2	Interferon lambda 2	Hs00265051_s5
	LTF	Lactotransferrin	Hs00265051_s6
	MX1	MX dynamin like GTPase 1	Hs00265051_s7
	SOCS3	Suppressor of cytokine signaling 3	Hs00265051_s8
Cell Signaling/Immune Cell Recruitment	*CCL2*	C-C motif chemokine ligand 2; MCP-1	Hs00265051_s9
	CCL3	C-C motif chemokine ligand 3; MIP-1-alpha	Hs00265051_s10
	CCL5	C-C motif chemokine ligand 5; RANTES	Hs00265051_s11
	CSF2	Colony stimulating factor 2; GM-CSF	Hs00265051_s12
	CXCL10	C-X-C motif chemokine ligand 10; IP-10	Hs00265051_s13
	CXCL11	C-X-C motif chemokine ligand 11	Hs00265051_s14
	CXCL8	C-X-C motif chemokine ligand 8; IL-8	Hs00265051_s15
	CXCL9	C-X-C motif chemokine ligand 9; MIG	Hs00265051_s16
	IL15	Interleukin 15	Hs00265051_s17
	IL1B	Interleukin 1 beta	Hs00265051_s18
	IL6	Interleukin 6	Hs00265051_s19
	TNF	Tumor necrosis factor	Hs00265051_s20
Mucins	*MUC5AC*	Mucin 5AC, oligomeric mucus/gel-forming	Hs00265051_s21
	MUC5B	Mucin 5B, oligomeric mucus/gel-forming	Hs00265051_s22
Surfactant (Surf.)	*SFTPA1*	Surfactant protein A1	Hs00265051_s23
	SFTPD	Surfactant protein D	Hs00265051_s24
Transcription Factors	*IRF1*	Interferon regulatory factor 1	Hs00265051_s25
	IRF3	Interferon regulatory factor 3	Hs00265051_s26
	IRF7	Interferon regulatory factor 7	Hs00265051_s27
	NFKB1	Nuclear factor kappa B subunit 1	Hs00265051_s28
	STAT1	Signal transducer and activator of transcription 1	Hs00265051_s29
	STAT2	Signal transducer and activator of transcription 2	Hs00265051_s30
	STAT3	Signal transducer and activator of transcription 3	Hs00265051_s31
Viral Recognition	*DDX58*	DExD/H-box helicase 58; RIG-I	Hs00265051_s32
	TLR3	Toll like receptor 3	Hs00265051_s33
	TLR7	Toll like receptor 7	Hs00265051_s34
	TLR9	Toll like receptor 9	Hs00265051_s35
Viral Genes	*nCoVN1*	SARS-CoV-2 Nucleocapsid	IDT Cat # 10006713
	nCoVN2	SARS-CoV-2 Nucleocapsid	IDT Cat # 10006713
Reference Genes	*GAPDH*	Glyceraldehyde-3-phosphate dehydrogenase	Hs00265051_s36
	ACTB	Actin beta	Hs00265051_s37
	RPP30	Ribonuclease P/MRP subunit P30	IDT Cat # 10006713

Table 3: Statistically significant particle-induced effects on gene expression in hNECs at 0, 24, and 72 h post (mock) infection. N=6 (3M, 3F) biological replicates per measurement.

Time	Gene	Category	Particle	Sex	Fold induction	p-value
0 h	IFNG	Antiviral Defense	DEP	Combined	0.06	2.30E-04
	TLR3	Viral Recognition	DEP	Combined	0.64	4.35E-04
	LTF	Antiviral Defense	Eucalyptus WSP	Combined	0.45	7.36E-04
	IL1B	Immune Cell Recruit.	Eucalyptus WSP	Combined	2.53	1.55E-03
	IL6	Immune Cell Recruit.	Eucalyptus WSP	Combined	5.29	6.63E-05
	TLR3	Viral Recognition	Eucalyptus WSP	Combined	0.60	5.88E-05
	IFNG	Antiviral Defense	Red Oak WSP	Combined	0.08	3.81E-04
	IL6	Immune Cell Recruit.	Red Oak WSP	Combined	5.53	5.08E-05
	TLR3	Viral Recognition	Red Oak WSP	Combined	0.56	6.43E-06
24 h	CTSB	Protease	Eucalyptus WSP	Combined	0.78	2.04E-03
	CCL2	Immune Cell Recruit.	Eucalyptus WSP	Combined	0.25	8.53E-04
	IL1B	Immune Cell Recruit.	Eucalyptus WSP	Combined	2.65	9.03E-04
	TMPRSS11D	Protease	Red Oak WSP	Combined	2.15	2.83E-03
	IL1B	Immune Cell Recruit.	Red Oak WSP	Combined	6.70	8.28E-10
72 h	MMP7	Protease	Red Oak WSP	Combined	0.39	3.32E-04
	IL1B	Immune Cell Recruit.	Red Oak WSP	Combined	2.42	2.73E-03

Table 4: Statistically significant virus-induced changes in gene expression in hNECs from males and females at 0, 24, and 72 h p.i. with SARS-CoV-2. N=9 biological replicates for individual sex effects (M or F) and N=18 for Combined effects.

Time	Gene	Function	Sex	Fold induction	p-value
0 h	TMPRSS11D	Protease	Combined	0.58	2.43E-03
	IFNG	Antiviral Defense	Combined	0.16	3.69E-03
	IFNG	Antiviral Defense	M	0.02	9.74E-05
	IFNG	Antiviral Defense	(#) M vs F	0.01	4.10E-04
	SFTPD	Surfactant	Combined	0.54	9.32E-05
	SFTPD	Surfactant	M	0.42	9.81E-05
24 h	IFNL1	Antiviral Defense	Combined	8.71	1.46E-04
	IFNL1	Antiviral Defense	M	20.68	1.92E-04
	IFNL2	Antiviral Defense	Combined	19.87	3.34E-05
	IFNL2	Antiviral Defense	M	20.86	2.07E-03
	STAT3	Transcription Factor	Combined	0.85	2.01E-03
	STAT3	Transcription Factor	F	0.80	1.63E-03
72 h	ACE2	Viral Entry Factor	Combined	2.42	1.00E-15
	ACE2	Viral Entry Factor	M	3.00	5.50E-13
	ACE2	Viral Entry Factor	F	1.95	1.89E-06
	CTSL	Protease	Combined	0.59	1.69E-09
	CTSL	Protease	M	0.58	6.90E-06
	CTSL	Protease	F	0.61	1.98E-05
	TMPRSS2	Protease	Combined	0.68	1.11E-05
	TMPRSS2	Protease	M	0.65	4.32E-04
	IFIT1	Antiviral Defense	Combined	26.04	1.00E-15
	IFIT1	Antiviral Defense	M	34.12	1.00E-15
	IFIT1	Antiviral Defense	F	19.87	1.00E-15
	IFITM3	Antiviral Defense	Combined	3.90	1.00E-15
	IFITM3	Antiviral Defense	M	4.69	1.00E-15
	IFITM3	Antiviral Defense	F	3.25	1.00E-15
	IFNB1	Antiviral Defense	Combined	21.33	1.00E-15
	IFNB1	Antiviral Defense	M	25.40	1.00E-15
	IFNB1	Antiviral Defense	F	17.91	1.00E-15
	IFNL1	Antiviral Defense	Combined	6936.06	1.00E-15
	IFNL1	Antiviral Defense	M	17769.31	1.00E-15
	IFNL1	Antiviral Defense	F	2707.41	1.00E-15
	IFNL2	Antiviral Defense	Combined	3694.08	1.00E-15
	IFNL2	Antiviral Defense	M	4439.86	3.20E-14
	IFNL2	Antiviral Defense	F	3073.57	1.60E-14
	LTF	Antiviral Defense	Combined	0.53	1.75E-04
	LTF	Antiviral Defense	F	0.48	1.62E-03
	MX1	Antiviral Defense	Combined	6.40	1.00E-15
	MX1	Antiviral Defense	M	7.95	1.00E-15
	MX1	Antiviral Defense	F	5.16	1.00E-15
	CCL3	Immune Cell Recruit.	Combined	23.01	1.00E-07
	CCL3	Immune Cell Recruit.	M	39.81	2.81E-05
	CCL3	Immune Cell Recruit.	F	13.31	3.10E-04
	CCL5	Immune Cell Recruit.	Combined	50.33	1.00E-15
	CCL5	Immune Cell Recruit.	M	80.16	1.00E-15

	CCL5	Immune Cell Recruit.	F	31.60	1.00E-15
	CXCL10	Immune Cell Recruit.	Combined	407.91	1.00E-15
	CXCL10	Immune Cell Recruit.	M	690.69	1.00E-15
	CXCL10	Immune Cell Recruit.	F	240.90	1.00E-15
	CXCL11	Immune Cell Recruit.	Combined	466.26	1.00E-15
	CXCL11	Immune Cell Recruit.	M	830.13	1.00E-15
	CXCL11	Immune Cell Recruit.	F	261.91	1.00E-15
	CXCL8	Immune Cell Recruit.	Combined	4.98	1.00E-15
	CXCL8	Immune Cell Recruit.	M	5.97	8.79E-12
	CXCL8	Immune Cell Recruit.	F	4.16	9.03E-09
	CXCL9	Immune Cell Recruit.	Combined	101.79	1.00E-15
	CXCL9	Immune Cell Recruit.	M	180.87	1.00E-15
	CXCL9	Immune Cell Recruit.	F	57.29	2.53E-11
	IL6	Immune Cell Recruit.	Combined	48.59	1.00E-15
	IL6	Immune Cell Recruit.	M	65.44	1.00E-15
	IL6	Immune Cell Recruit.	F	36.08	1.00E-15
	TNF	Immune Cell Recruit.	Combined	9.22	6.90E-14
	TNF	Immune Cell Recruit.	M	14.85	8.81E-11
	TNF	Immune Cell Recruit.	F	5.72	7.13E-06
	SFTPD	Surfactant	Combined	0.60	1.39E-03
	IRF1	Transcription Factor	Combined	1.49	3.15E-07
	IRF1	Transcription Factor	M	1.65	6.01E-06
	IRF3	Transcription Factor	Combined	0.83	1.10E-03
	IRF7	Transcription Factor	Combined	4.51	1.00E-15
	IRF7	Transcription Factor	M	5.34	1.00E-15
	IRF7	Transcription Factor	F	3.80	1.00E-15
	STAT1	Transcription Factor	Combined	3.40	1.00E-15
	STAT1	Transcription Factor	M	4.00	1.00E-15
	STAT1	Transcription Factor	F	2.89	1.00E-15
	STAT2	Transcription Factor	Combined	1.54	1.03E-07
	STAT2	Transcription Factor	M	1.85	1.23E-07
	STAT3	Transcription Factor	Combined	0.76	2.63E-07
	STAT3	Transcription Factor	M	0.76	3.35E-04
	STAT3	Transcription Factor	F	0.76	1.17E-04
	DDX58	Viral Recognition	Combined	6.41	1.00E-15
	DDX58	Viral Recognition	M	7.88	1.00E-15
	DDX58	Viral Recognition	F	5.21	1.00E-15
	TLR3	Viral Recognition	Combined	1.49	1.30E-05
	TLR3	Viral Recognition	M	1.67	8.77E-05
	TLR7	Viral Recognition	Combined	4.58	1.36E-05
	TLR7	Viral Recognition	M	9.12	1.06E-05
	TLR9	Viral Recognition	Combined	1.47	9.94E-04

Table 5: Statistically significant effects of particle exposure on virus-induced gene expression in hNECs at 0, 24, and 72 h p.i. N=6 (3M, 3F) biological replicates per measurement.

Time	Gene	Function	Particle	Sex	Fold induction	p-value
0 h	IRF1	Transcription Factor	DEP	Combined	0.64	3.61E-05
	IL1B	Immune Cell Recruit.	Eucalyptus WSP	Combined	2.55	1.38E-03
	IL6	Immune Cell Recruit.	Eucalyptus WSP	Combined	4.02	7.84E-04
	CTSB	Protease	Red Oak WSP	Combined	0.78	1.89E-03
	IL1B	Immune Cell Recruit.	Red Oak WSP	Combined	2.50	1.97E-03
	IL6	Immune Cell Recruit.	Red Oak WSP	Combined	8.52	5.59E-07
	STAT2	Transcription Factor	Red Oak WSP	Combined	0.72	3.40E-03
24 h	IL1B	Immune Cell Recruit.	DEP	Combined	3.53	2.78E-05
	IL1B	Immune Cell Recruit.	Eucalyptus WSP	Combined	3.69	1.13E-05
	CTSB	Protease	Red Oak WSP	Combined	0.74	1.45E-04
	FURIN	Protease	Red Oak WSP	Combined	0.71	2.30E-04
	MMP7	Protease	Red Oak WSP	Combined	0.41	7.24E-04
	MX1	Antiviral Defense	Red Oak WSP	Combined	0.66	1.68E-03
	IL1B	Immune Cell Recruit.	Red Oak WSP	Combined	3.30	6.47E-05
	STAT2	Transcription Factor	Red Oak WSP	Combined	0.69	8.85E-04
72 h	MMP7	Protease	Eucalyptus WSP	Combined	0.47	3.38E-03
	IFITM3	Antiviral Defense	Eucalyptus WSP	Combined	0.64	2.08E-04
	MX1	Antiviral Defense	Eucalyptus WSP	Combined	0.54	3.55E-06
	IL1B	Immune Cell Recruit.	Eucalyptus WSP	Combined	2.38	3.20E-03
	IRF7	Transcription Factor	Eucalyptus WSP	Combined	0.65	6.52E-04
	STAT1	Transcription Factor	Eucalyptus WSP	Combined	0.60	4.38E-06
	STAT2	Transcription Factor	Eucalyptus WSP	Combined	0.72	2.85E-03
	MMP7	Protease	Red Oak WSP	Combined	0.29	1.65E-05
	IFIT1	Antiviral Defense	Red Oak WSP	Combined	0.35	5.96E-06
	IFITM3	Antiviral Defense	Red Oak WSP	Combined	0.57	2.03E-05
	IFNB1	Antiviral Defense	Red Oak WSP	Combined	0.24	2.10E-06
	MX1	Antiviral Defense	Red Oak WSP	Combined	0.49	1.46E-06
	CCL3	Immune Cell Recruit.	Red Oak WSP	Combined	0.13	2.30E-03
	CCL5	Immune Cell Recruit.	Red Oak WSP	Combined	0.29	1.15E-03
	CXCL10	Immune Cell Recruit.	Red Oak WSP	Combined	0.19	9.47E-04
	CXCL11	Immune Cell Recruit.	Red Oak WSP	Combined	0.18	1.13E-03
	IRF7	Transcription Factor	Red Oak WSP	Combined	0.65	1.90E-03
	STAT1	Transcription Factor	Red Oak WSP	Combined	0.67	1.07E-03
	DDX58	Viral Recognition	Red Oak WSP	Combined	0.58	1.08E-03

Table 6: Statistically significant, sex-disaggregated effects of particle exposure on virus-induced gene expression in infected hNECs at 0, 24, and 72 h p.i. N=3 biological replicates per measurement.

Time	Gene	Function	Particle	Sex	Fold induction	p-value
0 h	IRF1	Transcription Factor	DEP	M	0.59	4.62E-04
	IL6	Immune Cell Recruit.	Red Oak WSP	M	8.77	2.41E-04
	IL6	Immune Cell Recruit.	Red Oak WSP	F	8.27	3.87E-04
	TLR3	Viral Recognition	Red Oak WSP	M	0.58	2.20E-03
24 h	IL1B	Immune Cell Recruit.	DEP	M	4.96	1.57E-04
	IL1B	Immune Cell Recruit.	Eucalyptus WSP	F	4.69	2.17E-04
	FURIN	Protease	Red Oak WSP	F	0.67	2.09E-03
	IL1B	Immune Cell Recruit.	Red Oak WSP	F	3.40	3.54E-03
72 h	IFITM3	Antiviral Defense	Eucalyptus WSP	F	0.56	5.88E-04
	MX1	Antiviral Defense	Eucalyptus WSP	F	0.43	8.25E-06
	IRF7	Transcription Factor	Eucalyptus WSP	F	0.52	3.29E-04
	STAT1	Transcription Factor	Eucalyptus WSP	F	0.49	7.24E-06
	STAT2	Transcription Factor	Eucalyptus WSP	F	0.62	1.97E-03
	MMP7	Protease	Red Oak WSP	M	0.22	4.72E-05
	IFIT1	Antiviral Defense	Red Oak WSP	F	0.18	1.63E-06
	IFITM3	Antiviral Defense	Red Oak WSP	F	0.41	9.25E-06
	IFNB1	Antiviral Defense	Red Oak WSP	F	0.13	6.06E-06
	MX1	Antiviral Defense	Red Oak WSP	F	0.32	3.90E-07
	MX1	Antiviral Defense	Red Oak WSP	(#) M vs F	2.35	2.96E-03
	CCL3	Immune Cell Recruit.	Red Oak WSP	M	0.07	1.60E-03
	CXCL10	Immune Cell Recruit.	Red Oak WSP	F	0.09	1.35E-03
	CXCL11	Immune Cell Recruit.	Red Oak WSP	F	0.08	1.05E-03
	IRF7	Transcription Factor	Red Oak WSP	F	0.45	1.98E-04
	STAT1	Transcription Factor	Red Oak WSP	F	0.52	3.37E-04
	DDX58	Viral Recognition	Red Oak WSP	F	0.40	3.60E-04